NAVAL POSTGRADUATE SCHOOL

MONTEREY, CALIFORNIA

THESIS

EFFECTS OF AIR INLET SWIRL ANGLE ON PERFORMANCE OF A TWO-STROKE DIESEL ENGINE

by

Jordan A. Klein

June 2018

Thesis Advisor: Garth V. Hobson
Co-Advisor: Douglas L. Seivwright

THIS PAGE INTENTIONALLY LEFT BLANK

REPORT DOCUMENTATION PAGE	*Form Approved OMB No. 0704-0188*

1. AGENCY USE ONLY *(Leave blank)*	**2. REPORT DATE** June 2018	**3. REPORT TYPE AND DATES COVERED** Master's thesis

4. TITLE AND SUBTITLE EFFECTS OF AIR INLET SWIRL ANGLE ON PERFORMANCE OF A TWO-STROKE DIESEL ENGINE	**5. FUNDING NUMBERS**
6. AUTHOR(S) Jordan A. Klein	
7. PERFORMING ORGANIZATION NAME(S) AND ADDRESS(ES) Naval Postgraduate School Monterey, CA 93943-5000	**8. PERFORMING ORGANIZATION REPORT NUMBER**
9. SPONSORING / MONITORING AGENCY NAME(S) AND ADDRESS(ES) Office of Naval Research, Arlington, VA 22203	**10. SPONSORING / MONITORING AGENCY REPORT NUMBER**

11. SUPPLEMENTARY NOTES The views expressed in this thesis are those of the author and do not reflect the official policy or position of the Department of Defense or the U.S. Government.

12a. DISTRIBUTION / AVAILABILITY STATEMENT Approved for public release. Distribution is unlimited.	**12b. DISTRIBUTION CODE** A

13. ABSTRACT (maximum 200 words)

Two-stroke diesel engines are a reliable, robust way to provide power in a multitude of naval applications, from electrical generators to construction equipment to marine propulsion. Improvement in the performance of such a common mechanical element would provide benefits in both reliability and cost effectiveness. Increasing the degree of air-fuel mixing in the cylinder prior to combustion is one such method of performance enhancement and is the method addressed by this research. The research model engine is a Detroit Diesel 3-53 two-stroke engine that utilizes a roots blower and eighteen circumferential holes in each cylinder for air intake and four valves in the cylinder head for exhaust. After performing a baseline run of the test engine, computational fluid analysis was performed on three engine configurations using ANSYS 18.2 CFX software. The cylinder models included one with intake holes in the original configuration, one in which the holes were given a 10 degree upward angle, and one in which the holes were angled 5 degrees farther to the left and 10 degrees upward. Results suggest that a configuration with a 10 degree upward angle of the intake holes will show a higher degree of mixing and increased overall performance.

14. SUBJECT TERMS two-stroke diesel, fluid analysis, swirl	**15. NUMBER OF PAGES** 65
	16. PRICE CODE

17. SECURITY CLASSIFICATION OF REPORT	**18. SECURITY CLASSIFICATION OF THIS PAGE**	**19. SECURITY CLASSIFICATION OF ABSTRACT**	**20. LIMITATION OF ABSTRACT**
Unclassified	Unclassified	Unclassified	UU

NSN 7540-01-280-5500 Standard Form 298 (Rev. 2-89) Prescribed by ANSI Std. 239-18

THIS PAGE INTENTIONALLY LEFT BLANK

Approved for public release. Distribution is unlimited.

EFFECTS OF AIR INLET SWIRL ANGLE ON PERFORMANCE OF A TWO-STROKE DIESEL ENGINE

Jordan A. Klein
Lieutenant, United States Navy
BS, Texas A & M University, 2010

Submitted in partial fulfillment of the
requirements for the degree of

MASTER OF SCIENCE IN MECHANICAL ENGINEERING

from the

NAVAL POSTGRADUATE SCHOOL
June 2018

Approved by: Garth V. Hobson
Advisor

Douglas L. Seivwright
Co-Advisor

Garth V. Hobson
Chair, Department of Mechanical and Aerospace Engineering

THIS PAGE INTENTIONALLY LEFT BLANK

ABSTRACT

Two-stroke diesel engines are a reliable, robust way to provide power in a multitude of naval applications, from electrical generators to construction equipment to marine propulsion. Improvement in the performance of such a common mechanical element would provide benefits in both reliability and cost effectiveness. Increasing the degree of air-fuel mixing in the cylinder prior to combustion is one such method of performance enhancement and is the method addressed by this research. The research model engine is a Detroit Diesel 3-53 two-stroke engine that utilizes a roots blower and eighteen circumferential holes in each cylinder for air intake and four valves in the cylinder head for exhaust. After performing a baseline run of the test engine, computational fluid analysis was performed on three engine configurations using ANSYS 18.2 CFX software. The cylinder models included one with intake holes in the original configuration, one in which the holes were given a 10 degree upward angle, and one in which the holes were angled 5 degrees farther to the left and 10 degrees upward. Results suggest that a configuration with a 10 degree upward angle of the intake holes will show a higher degree of mixing and increased overall performance.

THIS PAGE INTENTIONALLY LEFT BLANK

TABLE OF CONTENTS

I. INTRODUCTION....1

II. BASELINE ANALYSIS OF DETROIT DIESEL 3-53....3
- **A. ENGINE CHARACTERISTICS....3**
- **B. BASELINE TESTING....4**
  - **1. Setup....4**
  - **2. Data Acquisition and Analysis....5**
  - **3. Procedure....6**
- **C. RESULTS AND DISCUSSIONS....8**
  - **1. Power....8**
  - **2. Torque....10**
  - **3. BSAC....10**
  - **4. BSFC....12**
  - **5. Thermal Efficiency....13**
  - **6. Pressure-Volume Diagrams....13**

III. DESIGN....17
- **A. BACKGROUND....17**
- **B. APPROACH....17**
  - **1. Baseline Configuration (Case 1)....19**
  - **2. Increased Vertical Angle (Case 2)....19**
  - **3. Increased Vertical, Reduced Horizontal Angle (Case 3)....20**
- **C. MODELING....21**

IV. COMPUTATIONAL FLUID ANALYSIS....23
- **A. MODEL SETUP....23**
  - **1. Geometry and Meshing....23**
  - **2. Solver Constraints....23**
- **B. RESULTS....26**
  - **1. Mass Flow Rate....26**
  - **2. Mixing....27**
  - **3. Pressure Ratio....34**
- **C. COMPARISON....36**

V. CONCLUSIONS....37

APPENDIX. MATLAB CODE....39

A. SI UNITS.....39
B. ENGLISH UNITS.....42

LIST OF REFERENCES.....47

INITIAL DISTRIBUTION LIST.....49

LIST OF FIGURES

Figure 1. Schematic of Detroit Diesel 3-53 Cylinder. Source: [5]. 3

Figure 2. Detroit Diesel 3-53 Performance Map. Source: [6]. 7

Figure 3. Power and Torque Versus Speed (SI Units) 9

Figure 4. Power and Torque Versus Speed (English Units) 9

Figure 5. BSAC Versus Speed (SI Units) 11

Figure 6. BSAC Versus Speed (English Units) 11

Figure 7. BSFC and Thermal Efficiency Versus Speed (SI Units) 12

Figure 8. BSFC and Thermal Efficiency Versus Speed (English Units) 13

Figure 9. Pressure-Volume Diagram (SI Units) 14

Figure 10. Pressure-Volume Diagram (English Units) 15

Figure 11. Detroit Diesel 3-53 Cylinder Liner 18

Figure 12. Original Intake Hole Orientation 19

Figure 13. Side View of Upward Angled Intake Slot 20

Figure 14. Top View of Slot with Increased Vertical Angle and Reduced Horizontal Angle 21

Figure 15. Momentum Display Monitors for Case 1 25

Figure 16. Momentum Display Monitors for Case 2 25

Figure 17. Momentum Display Monitors for Case 3 26

Figure 18. Velocity Streamlines for Case 1 27

Figure 19. Velocity Swirl Strength in YZ plane for Case 1 28

Figure 20. Velocity Swirl Strength in YZ plane for Case 2 29

Figure 21. Velocity Swirl Strength in YZ plane for Case 3 29

Figure 22. Velocity Swirl Strength in XZ Plane for Case 1 30

Figure 23. Velocity Swirl Strength in XZ Plane for Case 2.....31
Figure 24. Velocity Swirl Strength in XZ Plane for Case 3.....31
Figure 25. Velocity Swirl Strength Vectors for Case 1.....32
Figure 26. Velocity Swirl Strength Vectors for Case 2.....33
Figure 27. Velocity Swirl Strength Vectors for Case 3.....33
Figure 28. Vertical Pressure Contour for Case 1.....34
Figure 29. Vertical Pressure Contour for Case 2.....35
Figure 30. Vertical Pressure Contour for Case 3.....35

LIST OF TABLES

Table 1. Detroit Diesel 3-53 Engine Characteristics. Adapted from [4], [5]. 4

Table 2. Detroit Diesel 3-53 Performance Specifications. Adapted from[4], [5]. 4

Table 3. Cylinder 1 Work Per Cycle at Various Speeds 15

Table 4. RMS Residual Values 24

THIS PAGE INTENTIONALLY LEFT BLANK

LIST OF ACRONYMS AND ABBREVIATIONS

a	Crank Radius
B	Bore
BDC	Bottom Dead Center
BSAC	Brake Specific Air Consumption
BSFC	Brake Specific Fuel Consumption
CAD	Computer Aided Design
D	Diameter
DAQ	Data Acquisition System
l	Crank Rod Length
LHV	Lower Heating Value
μ	Dynamic Viscosity
NPS	Naval Postgraduate School
OEM	Original Equipment Manufacturer
P	Power
Q	Heat
RMS	Root Mean Squared
RPM	Revolutions Per Minute
Re	Reynolds' Number
ρ	Density
TDC	Top Dead Center
τ	Torque
θ	Crank Angle
W	Work
ω	Angular Velocity
V	Volume
Vc	Clearance Volume

THIS PAGE INTENTIONALLY LEFT BLANK

I. INTRODUCTION

Diesel engine technology has been a reliable, robust source of power since its inception with Rudolf Diesel's development of a theoretical compression-ignition cycle in 1892 and prototype production in 1897. It sees usage in applications ranging from farm machinery to large marine vessels. The United States Navy currently uses diesel engines for main propulsion in six commissioned ship classes and for auxiliaries in many more. Much of the Navy's heavy equipment also utilizes diesel technology.

Diesel technology has matured greatly and sees life in many configurations. The two main classes of these engines are two-stroke and four strokes. While the four-stroke engine maintains a separate stroke for each process in an internal combustion engine (intake, compression, combustion and expansion), a two-stroke engine combines the intake and exhaust as a single process at the end of the downstroke [1]. Two-stroke engines provide a high power-to-weight ratio and simplicity compared with four-stroke versions but tend to operate efficiently over a narrower range of speeds. Hence, methods of improving the power, torque, and efficiency of two-stroke engines are of great interest.

Many methods of performance enhancement have been studied for two-stroke diesels. Some methods focus on improving scavenging (the air intake-exhaust process) through means like intake and exhaust port location and arrangement and opposing cylinders [1]. Other methods utilize supercharging or turbocharging, wherein air induction is forced either mechanically or by an exhaust turbine respectively. One proposed model utilizes additional compression and expansion cylinders to provide higher efficiency [2]. Research on more effective and cleaner fuels is extensive and ongoing. However, one area that bears further investigation is the airflow pattern within the cylinder.

Modern advances in fluid modeling have made analysis and manipulation of airflow characteristics a promising option for increasing engine performance. Study of the velocity and swirl patterns within the cylinder was started in 1983 with Sung, Laitone and Patterson's analysis of velocity fields in the region of the air intake slots of a Detroit Diesel 6V-92 engine [3]. Using the random vortex method in two planes, they found that as flow

developed swirl began in the inlet direction, then became asymmetric and unsteady. This swirling, unsteady flow provides a potential method for efficiency improvement. If the swirl and flow patterns of the air can be manipulated, a more homogeneous air-fuel mixture can be obtained, improving complete combustion. In turn, more efficient combustion leads to more power per stroke and a more effective engine.

The most direct way to affect the flow of air in the cylinder is to alter the way in which it enters. Varying the angle and area of the air intake will inevitably provide different flow patterns, but exactly how these parameters affect flow has not, until now, been extensively studied. By providing analysis of the effects of different intake slot arrangements, this thesis will build the foundation for enhancement in the performance of two-stroke diesel engines.

II. BASELINE ANALYSIS OF DETROIT DIESEL 3-53

A. ENGINE CHARACTERISTICS

The Detroit Diesel 3-53 is a three-cylinder, two stroke diesel engine. Air enters the cylinder through eighteen evenly spaced, circumferentially arranged intake slots when the piston is at Bottom Dead Center position, as shown in Figure 1. The procedure and schematics in Petersen [4] describe how as the piston moves upward, the air reaches sufficient pressure and temperature to ignite the fuel as it is injected near the top of the stroke. Combustion drives the piston downward and as it nears the end of the downstroke, exhaust valves open to allow the products of combustion to escape. The engine characteristics of the 3-53 are found in Table 1 and ideal performance specifications are found in Table 2.

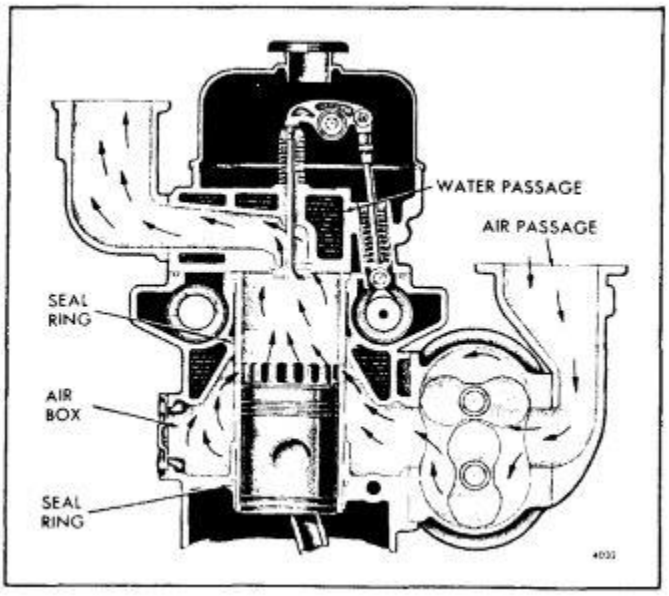

Figure 1. Schematic of Detroit Diesel 3-53 Cylinder. Source: [5].

Table 1. Detroit Diesel 3-53 Engine Characteristics.
Adapted from [4], [5].

Connecting Rod Length	22.352 cm (8.8 in)
Bore	9.8425 cm (3.875 in)
Stroke	11.43 cm (4.5 in)
Clearance Volume	42.15 cm^3 (2.5721 in^3)
Compression Ratio	21:1
Displacement	868.5 cm^3 (53 in^3) per cylinder
Valves/cylinder	4
Valve Lift	1.006 cm (0.3962 in)

Table 2. Detroit Diesel 3-53 Performance Specifications.
Adapted from [4], [5].

Power	69 kW (92 hp)
Maximum Speed	2800 RPM
Peak Torque	268.45 N-m (198 ft-lbf) at 1500 RPM
Mean Effective Pressure	579 kPa (83 psi)
Charge Feeding Pressure	27.6 kPa (4 psid)

B. BASELINE TESTING

The first step in the analysis of how air inlet angle affects an engine's performance was establishing baseline data. While manufacturer's data is a useful estimate of engine operating characteristics, each individual engine will differ slightly from theoretical specifications. In order to provide a legitimate analysis of how performance is affected by fuel-air mixing due to different installed fuel injectors, baseline data collection was performed on the NPS Diesel Propulsion engine.

1. Setup

The specific diesel engine used for testing was a refurbished model located on a test stand in the NPS Marine Propulsion Laboratory. It was connected to a SuperFlow SF-901 water brake dynamometer for power and torque absorption. Diesel II with a LHV of 43.2 MJ/kg (18,573 BTU/lbm) was used as the fuel.

2. Data Acquisition and Analysis

In order to provide a full and accurate assessment of the engine's actual operating characteristics, it was necessary to collect and calculate a number of direct and derived measurements. This task was accomplished through the use of the SuperFlow WinDyn Data Acquisition System and the Engine Cycle Analyzer high-speed acquisition system.

a. SuperFlow Data

The SuperFlow SF-901 DAQ measured a wide array of operating parameters. Using direct measurements, engine power was calculated with torque and angular velocity using the formula

$$P = \tau \times \omega$$

Specific fuel consumption and brake specific air consumption were derived from flow measurement data to provide information on the amount of fuel and air required to deliver power from the engine. Essentially, these parameters measure the fuel and air as a function of the power delivered at specified operating points. The SuperFlow DAQ measured air and fuel flow rate so that BSFC and BSAC were calculated with the following formulas respectively:

$$BSFC = \frac{\dot{m}_f}{P_{shaft}}$$

$$BSAC = \frac{\dot{m}_a}{P_{shaft}}$$

Thermal efficiency is a comparison of the engine's power output to its heat input. This value expresses what percentage of the energy delivered to the engine is actually transformed into mechanical work. Functionally, the heat input is assumed to be the product of the mass flow rate of the fuel and the energy density or Lower Heating Value of the fuel. Using the calculated power, measured fuel rate and LHV of the fuel, thermal efficiency was calculated using the formula:

$$\eta_{th} = \frac{W_{out}}{Q_{in}} = \frac{P}{LHV \times \dot{m}_f}$$

b. Engine Cycle Analyzer

The SNERGY v4.2 Engine Cycle Analyzer provided pressure data for each cylinder on a per-cycle basis. It provided an instantaneous cylinder pressure for crank angles of -180 degrees to 180 degrees in 0.5 degree increments. Using the relationships between clearance volume (Vc), cylinder bore (B), crank radius (a), connecting rod length (l), and crank angle (θ), the cylinder volume was calculated at each data point using the formula:

$$V = V_c + \frac{\pi * (B)^2}{4}(l + a - \left(a * cos\theta - \sqrt{l^2 - a^2 * sin^2\theta}\right))$$

Pressure-Volume curves for each cylinder were generated with these volumes at each operating condition using MATLAB R2017a software. From each curve, gas work per engine cycle was calculated from the area inside the curve. The area integral necessary for calculation was approximated by applying the trapezoidal rule. To provide power values for comparison with the SuperFlow data, gas work for each cylinder was summed and the collective value multiplied by speed at each operating condition

3. Procedure

To establish the characteristics of the NPS diesel, the engine was started and brought to idle. The operators then brought the engine to four separate operating points, attempting to match the manufacturer's power and torque curves as displayed in Figure 2.

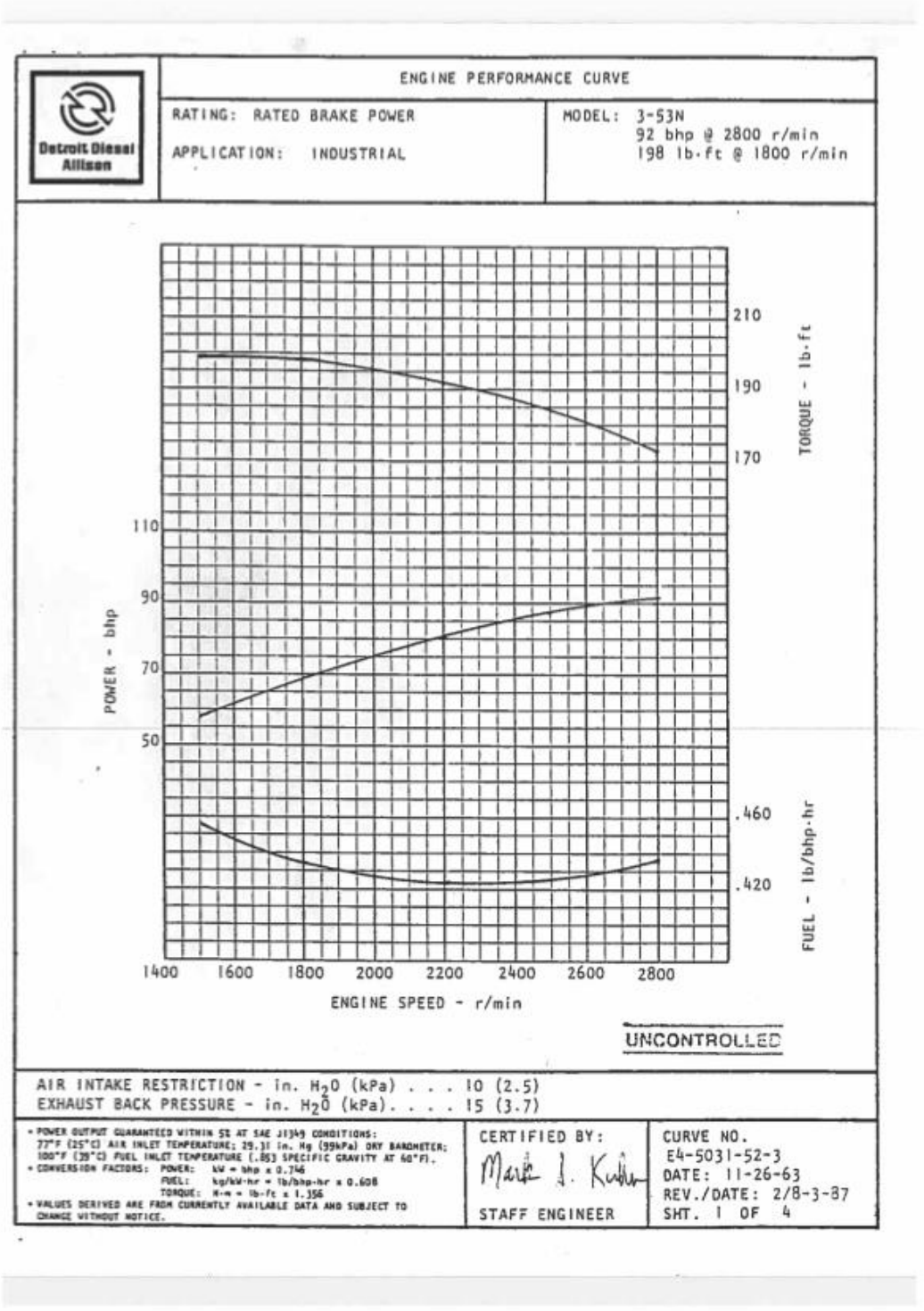

Figure 2. Detroit Diesel 3-53 Performance Map. Source: [6].

Idle conditions of 560 RPM and 40.67 N-m (30 ft-lbf) of torque were maintained until the engine reached operating temperature. The engine was then brought to an operating speed of 1600 RPM and allowed to reach steady state. Once the engine had stabilized, dynamometer data was collected from the DAQ and the process was repeated at 2180 RPM, 2500 RPM, and 2580 RPM. Engine Cycle Analysis data was collected at 560 RPM, 1600 RPM, 2200 RPM, 2500 RPM, and 2600 RPM. The engine was then shut down and data exported for analysis.

C. RESULTS AND DISCUSSIONS

The data obtained from the DAQ and ECA are useful measures of how the NPS Marine Propulsion 3-53 operated in comparison to the rated performance. While exact parameter values differed, the NPS diesel followed similar trends to manufacturer specified operation.

1. Power

The power curves shown in Figures 3 and 4 show the behavior of increasing power with higher speed. Along each curve, power increased to a maximum at approximately 2500 RPM then begins to decrease at higher speeds. At higher speeds, volumetric efficiency of the engine decreases, decreasing the supplied torque as a result of airflow losses in the intake ports and valves as well as mechanical losses which are predominant at higher speeds. Power will continue to increase as it is a product of torque and speed but will peak due to the decreasing effects of torque. The measured power curve shows a sharper decrease than the supplied curve differing by 14.7% at maximum power. Mechanical losses of friction, wear and differences in fuel and maintenance prevent the NPS engine from providing the rated performance for a newly rated engine.

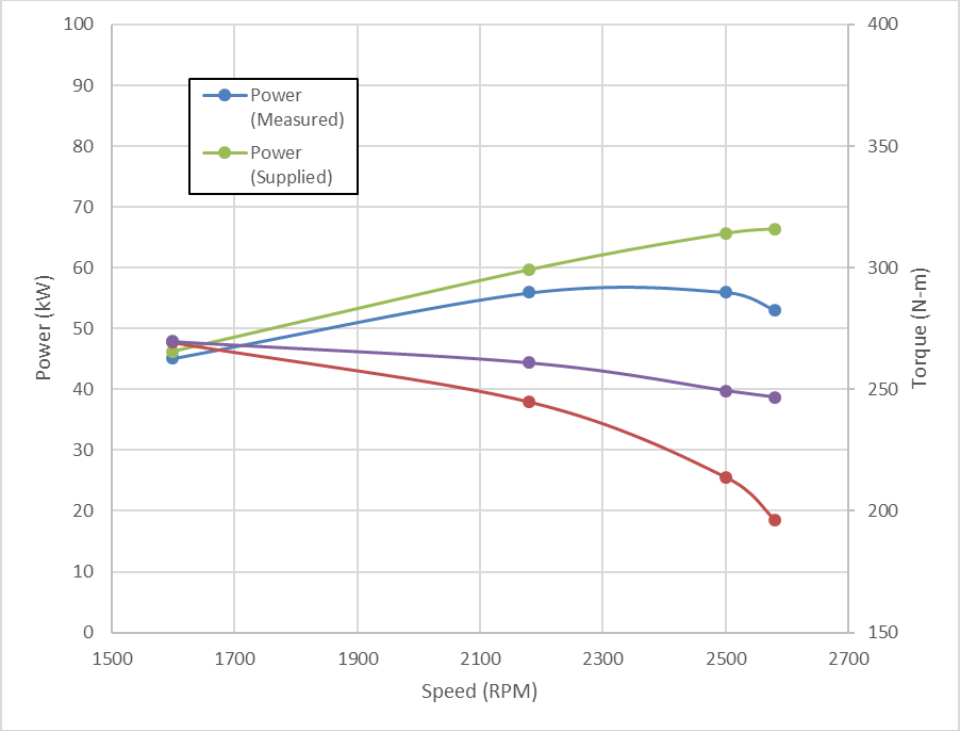

Figure 3. Power and Torque Versus Speed (SI Units)

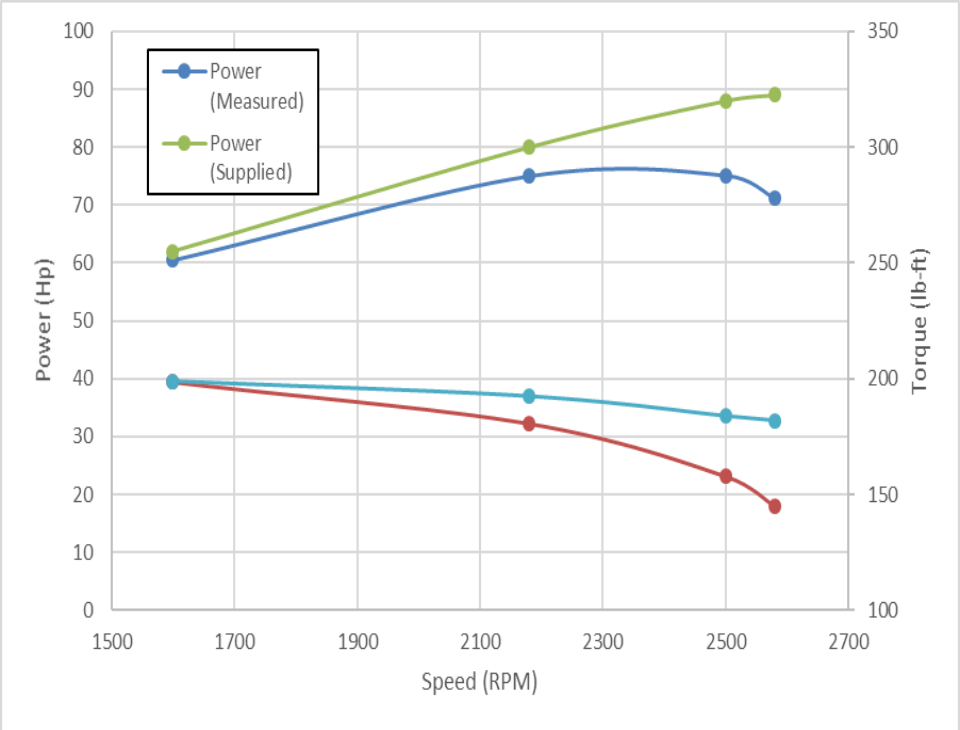

Figure 4. Power and Torque Versus Speed (English Units)

2. Torque

The theoretical and measured torque values both decrease with increasing speed. Maximum torque values of 269.4 N-m (198.7lb-ft) and 269.8 N-m (199lb-ft) for measured and theoretical curves, respectively, occurred at the lowest measured speed of 1600 RPM. The measured torque values of the test engine decreased more at higher speeds, showing a 27.2% reduction from 1600 to 2580 RPM while the manufacturer data showed only an 8.5% decrease. Noticeably, the difference in measured and theoretical performance was higher at higher speeds as well, indicating that the NPS diesel deviated more from rated performance at increased RPM. This deviation supports the conclusion that mechanical losses like friction and incomplete combustion that play a greater role at high speed were larger for the test engine than the manufacturer's rated model.

3. BSAC

The BSAC values in Figures 5 and 6 show how the engine required dramatically more airflow to deliver power at higher speeds. While higher power was available at higher speeds, the air demanded for that power was also dramatically higher. From 2200 to 2500 RPM, power increased only 0.13% while BSAC increases 12.4%. From this pattern it was clear that mid-range speeds provided the greatest balance of power delivery and air demand. Again, the BSAC trends reinforce the analysis that mechanical losses at higher speeds were the limiting factor in engine performance.

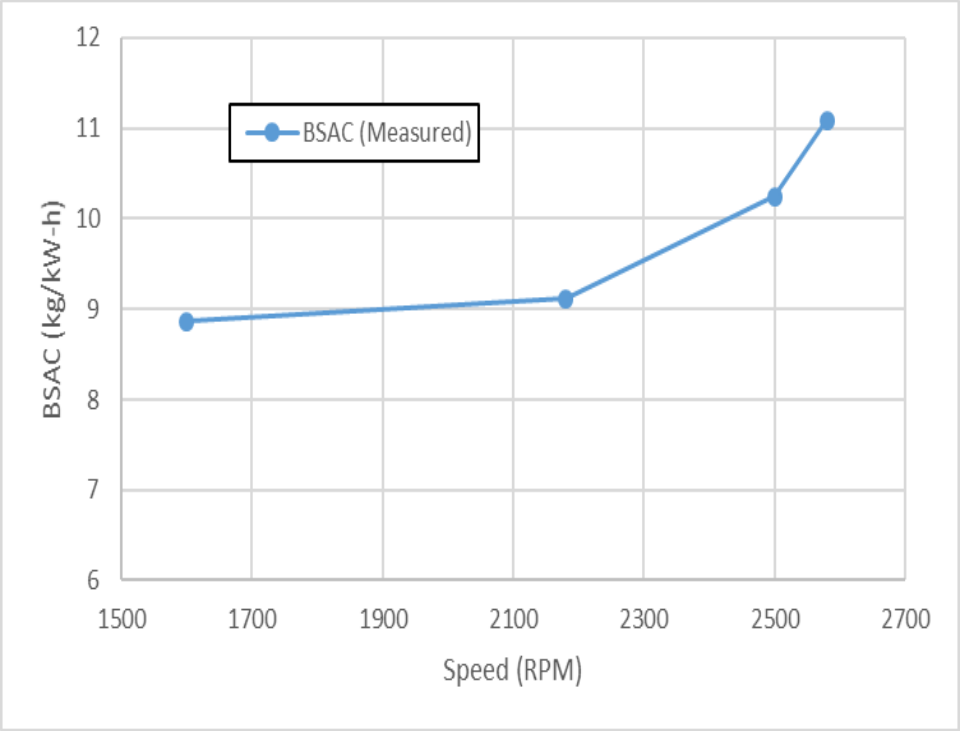

Figure 5. BSAC Versus Speed (SI Units)

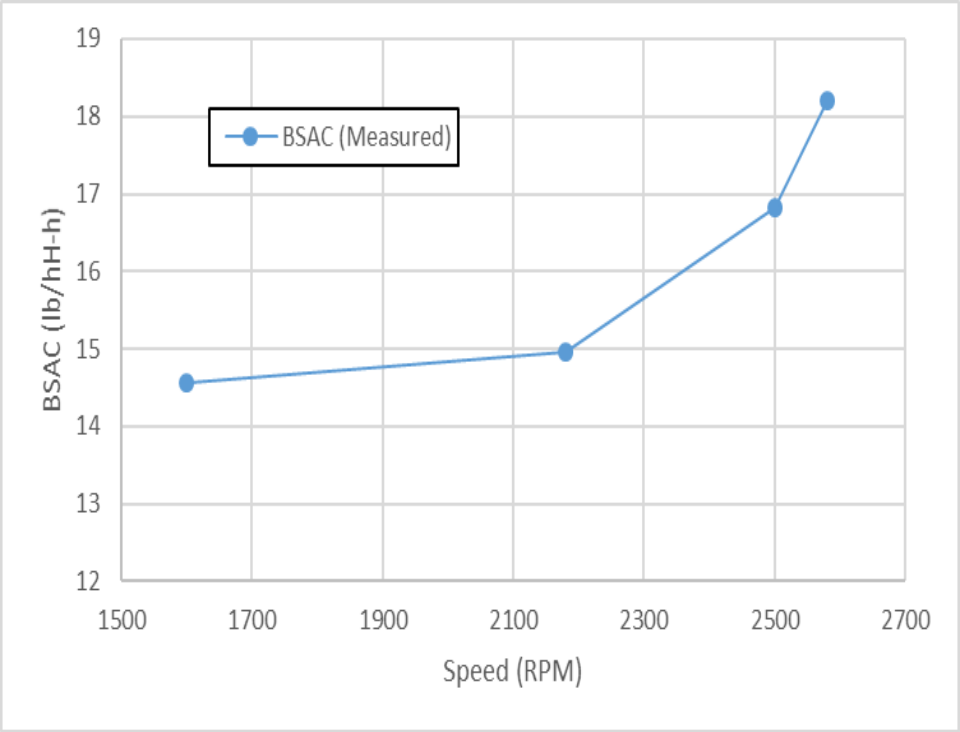

Figure 6. BSAC Versus Speed (English Units)

4. BSFC

Both measured and supplied BSFC curves decreased initially to a minimum at 2180 RPM then begin to rise. At this speed, the engine was operating slowly enough for complete, efficient combustion but quickly enough to deliver a high number of power strokes; slower operation allowed combustion but reduced the number of power cycles while faster operation limited the combustion process so less power was delivered per stroke. The measured curve rises much more steeply, however, in keeping with the trend in power generation; experimental power decreased more quickly at high speeds which decreased the denominator of the BSFC equation and raised its value. Comparatively, the NPS engine delivered less power for a given fuel flow rate. However, the difference in fuel consumption is comparatively small, with the experimental engine consuming a maximum of 12.9% more fuel.

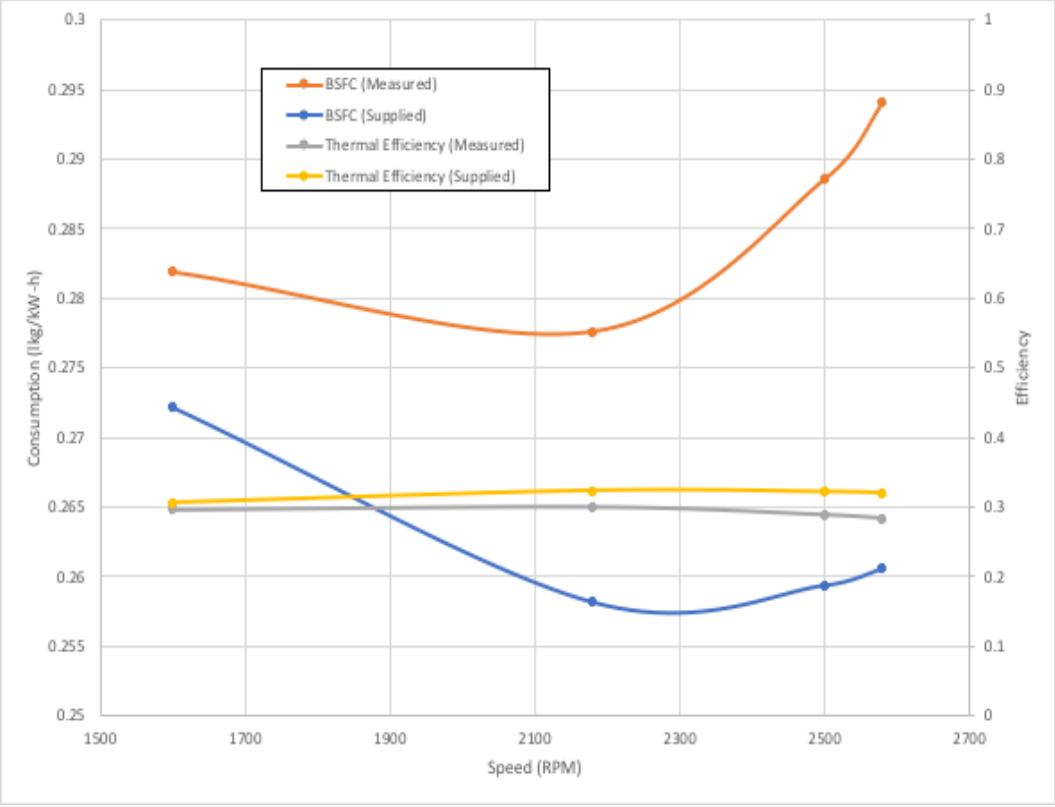

Figure 7. BSFC and Thermal Efficiency Versus Speed (SI Units)

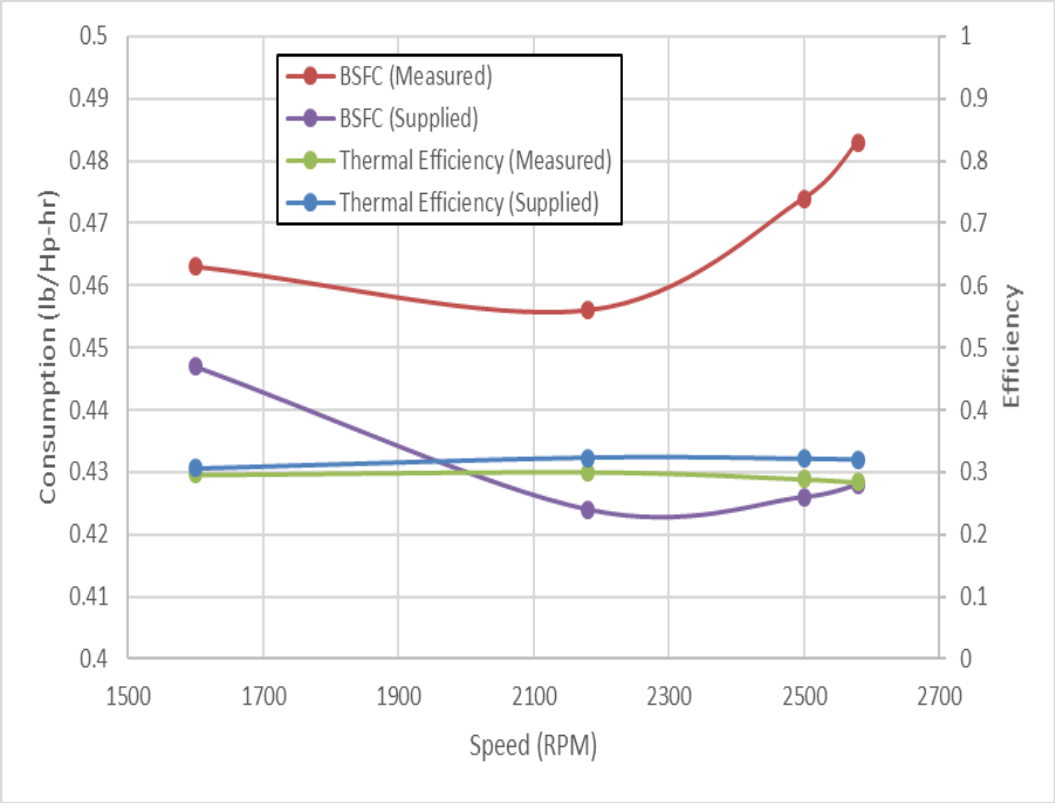

Figure 8. BSFC and Thermal Efficiency Versus Speed (English Units)

5. Thermal Efficiency

The thermal efficiency trends shown in Figures 7 and 8 are closely related to the trends in BSFC. Both measured and theoretical curves show the highest efficiency, or amount of work delivered for heat input, at 2180 RPM. The thermal efficiency curves are very close in value, hovering around 0.30 in both the Detroit manufacturer data and test engine. Thermal losses, therefore, do not appear to be the reason for differences in power and fuel consumption; mechanical losses are the more likely culprit.

6. Pressure-Volume Diagrams

Diagrams of pressure versus volume shown in Figures 9 and 10 display the range of pressures reached throughout a single piston cycle. The data presented is for Cylinder 1; data for Cylinders 2 and 3 showed similar trends. Notably, the engine reached its highest pressures at 2200 RPM, the speed of greatest thermal efficiency. Comparing the values of

work per cycle in Table 3 demonstrates the reason behind the peak efficiency at midrange speed. At 2200 RPM, the average work per cycle, 0.7529MJ (0.2805 hp-h) was the highest of any speed. Functionally, the engine was delivering the greatest amount of work per stroke.

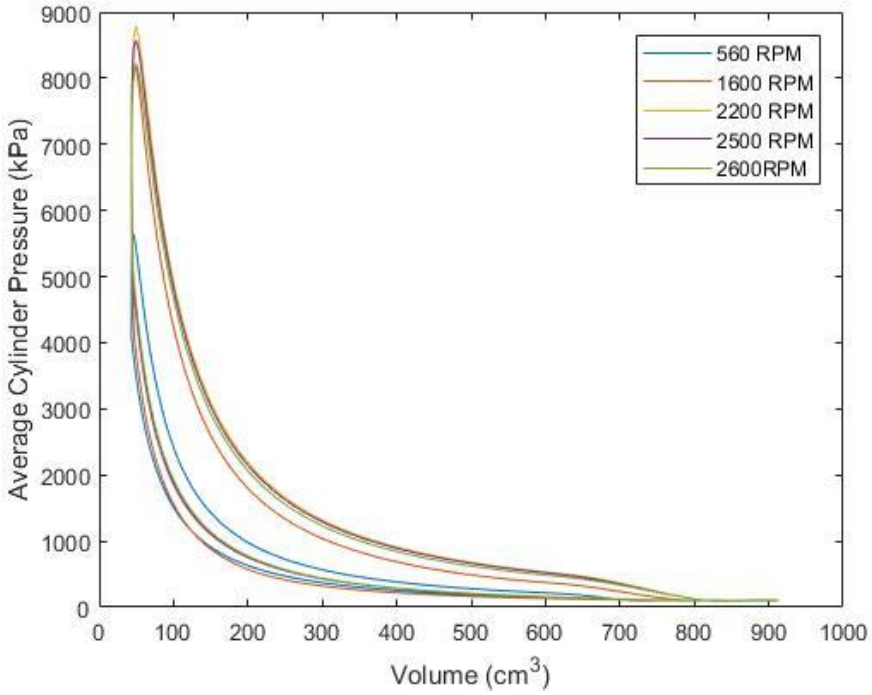

Figure 9. Pressure-Volume Diagram (SI Units)

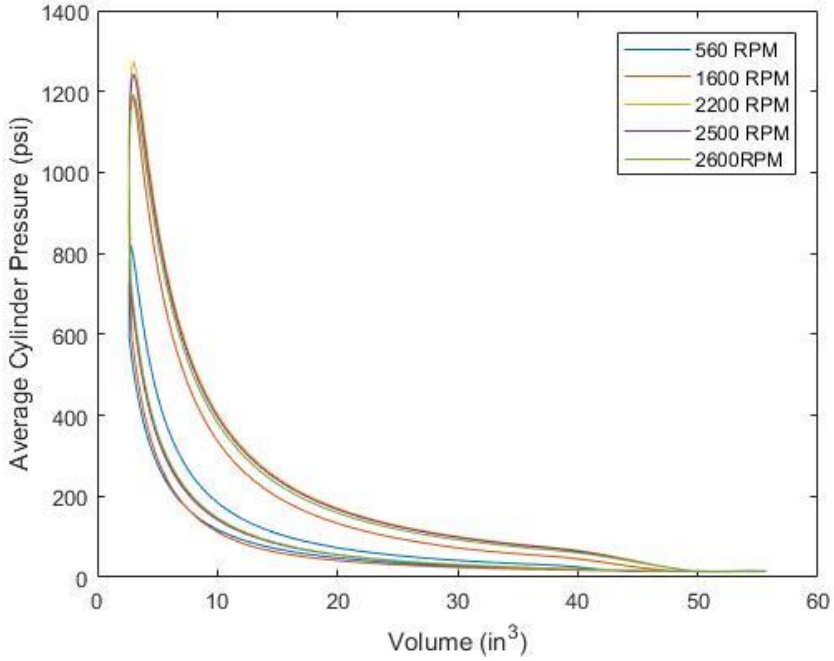

Figure 10. Pressure-Volume Diagram (English Units)

Table 3. Cylinder 1 Work Per Cycle at Various Speeds

Speed	Work/Cycle
RPM	MJ (hp-hr)
560	0.1993 (0.0742)
1600	0.623 (0.2321)
2200	0.7529 (0.2805)
2500	0.7269 (0.2708)
2600	0.6675 (0.2487)

On the whole, baseline analysis demonstrates how the NPS diesel engine follows the expected behavior of a diesel engine but deviates from the manufacturer's specifications due to friction and mechanical losses.

THIS PAGE INTENTIONALLY LEFT BLANK

III. DESIGN

A. BACKGROUND

One of the more effective methods for improving performance is increasing the degree of air-fuel mixing within the cylinder. Since this parameter cannot be controlled directly, the best way to approach mixing is through the airflow characteristics within the cylinder.

Air mass flow rate is the most straightforward and easily measured parameter to affect air-fuel mixing. An increase in flow rate, assuming constant density, indicates an increase in velocity. Higher velocity is accompanied by higher turbulence as measured by Reynolds' number:

$$Re = \frac{\rho \times V \times D}{\mu}$$

Higher turbulence will cause greater interaction between the airstream and the fuel droplets.

Outlet to inlet pressure ratio averaged by mass flow rate is an excellent indicator of the resistance to flow through the cylinder as a whole. A higher pressure ratio indicates that the air is not passing as easily through the cylinder; consequently, it is spending more time within the cylinder boundary and has more opportunity to mix with fuel before combustion. Altering this pressure ratio is another opportunity to improve air-fuel mixing within the cylinder.

Perhaps the most tangible way to manipulate the air-fuel mixing is by changing the path of the air through the cylinder. Increasing or decreasing the amount of swirl the air undergoes in its path to the exhaust valves will affect the amount of fuel spray it interacts with and the dispersion of that fuel prior to combustion.

B. APPROACH

The hardened alloy cast iron cylinder liner of a Detroit Diesel 3-53, shown in Figure 11, provides the boundary between the combustion chamber and the engine block itself [7].

It includes eighteen slots spaced evenly around the circumference of the liner that allow air from the roots blower to flow into the cylinder during intake.

Figure 11. Detroit Diesel 3-53 Cylinder Liner

Adjusting the angle of the intake slots of the cylinder was a major consideration of this thesis. As the inlet angle changes, the slotted area open to flow (when the piston is at BDC) is altered, thereby affecting mass flow rate as interference is adjusted up or down. Changing the inlet angle will also change the flow path of the air particles through the cylinder, giving them a more or less tortuous path en route to the exhaust ports. Consequently, the amount of swirl and pressure ratio will change as well.

In order to conduct a thorough analysis of precisely how inlet angle affected each one of these measurements, three cases were selected for comparison.

1. Baseline Configuration (Case 1)

The liner included eighteen slots located 9.576 cm (3.77 in) from the top of the cylinder liner. Each slot has two semicircular ends with radii of 0.635 cm (0.250 in) and center to center distance of 0.871 cm (0.343 in).

In the original manufacturing design, each hole is level with respect to the top of the cylinder (i.e., horizontal)and angled 19.09 degrees to the right of a line normal to the cylinder's surface as shown in Figure 12.

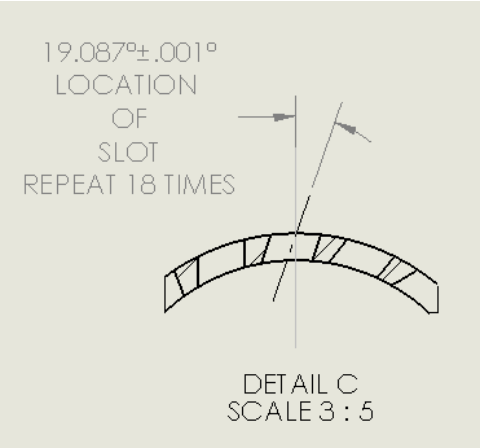

Figure 12. Original Intake Hole Orientation

When the piston is at BDC, air flows from the roots blower through the slots and into the cylinder. At this point, 0.212 cm^2 (0.0329 in^2) of the slot is obstructed by the cylinder, meaning approximately 91% of the slot's area is open to flow into the cylinder.

This configuration will be referred to hereafter as Case 1.

2. Increased Vertical Angle (Case 2)

The first test configuration for improved air-fuel mixing is the addition of a 10 degree angle toward the top of the cylinder liner for each intake slot, displayed in Figure 13. In this configuration the airflow is directed vertically toward the top of the cylinder requiring a less tortuous path to the top of the cylinder and fuel spray.

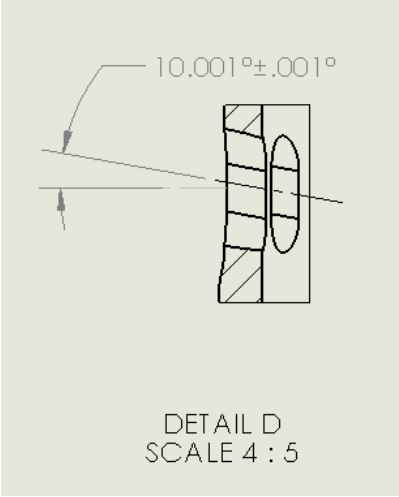

Figure 13. Side View of Upward Angled Intake Slot

In addition, piston interference with intake area is reduced due to the upward angle of the slot. At BDC the piston covers only 0.029 cm^2 (0.0045 in^2) of the slot area, leaving 98.8% of the area open to flow. \

This configuration will be referred to hereafter as Case 2.

3. Increased Vertical, Reduced Horizontal Angle (Case 3)

The second test design was a slot with a 10 degree upward angle but a 5 degree reduction of horizontal angle, totaling 14.09 degrees right of the surface normal as shown in Figure 14.

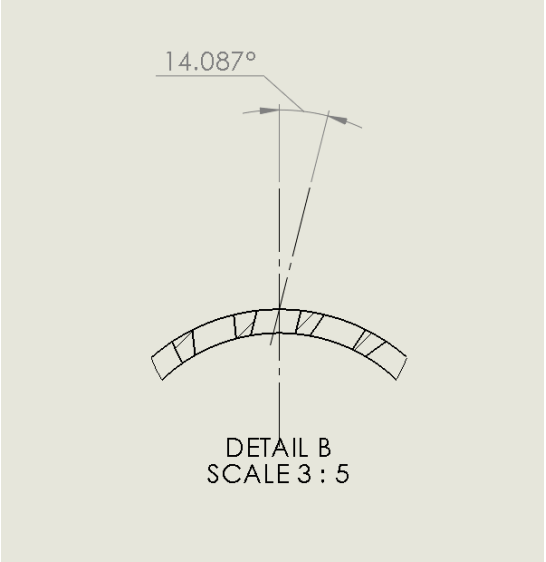

Figure 14. Top View of Slot with Increased Vertical Angle and Reduced Horizontal Angle

This configuration shares the same piston interference area as Case 2, but directs the flow more toward the center of the cylinder. A more shallowly directed flow will create more streamline interference upon air intake and prospectively increase the degree of mixing within the cylinder.

C. MODELING

Calipers were used to take measurements of all vertical, horizontal and radial dimensions. Determining the location and angle of the intake slots was a more complex process. A Coordinate Measuring Machine arm was used to generate points in three-dimensional space along the profile of the slots. The relation of these points provided the internal dimensions and angles of the holes. These dimensions were subsequently used to create three SolidWorks 2017 CAD models of the liner, two of which were altered with the appropriate inlet angles for Case 2 and 3.

Basic dimensions of the piston were taken with calipers. In order to develop a digital model of the piston head, depth measurements were taken at seventeen separate points along the top of the cylinder. These coordinate measurements were used to develop

an accurate profile curve for the SolidWorks 2017 model of the piston. Valves were also measured and replicated in digital form.

In order to create a boundary for flow analysis, a CAD model of the liner and internal cylinder volume was added to a cylinder of height and radius with a rectangular prism to simulate the inlet area from the roots blower. Solid models of the exhaust ports were added to the top to generate a total flow volume for fluid flow analysis.

IV. COMPUTATIONAL FLUID ANALYSIS

A. MODEL SETUP

Flow rate and air-fuel mixing are two of the most important parameters in determining the efficiency of an internal-combustion engine. While there are a number of ways to alter these parameters, the focus of this project was to study the effects of altering the angle of air inlets in the cylinder liner of a Detroit Diesel 3-53 engine. Three possible orientations were studied; Case 1 was the baseline configuration with no vertical angle and 19.09 degrees to the right when viewed from above. Case 2 had the same horizontal angle and a 10 degree vertical angle, while Case 3 included a 5 degree reduction in horizontal angle (14.09 degrees total). In order to conduct the comparison, flow through the cylinder was measured for each case in the CFX module of ANSYS Workbench 18.2 and analyzed in terms of mass flow rate, velocity swirl strength (mixing), and mass-averaged pressure ratio from inlet to outlet.

1. Geometry and Meshing

The first step in conducting the analysis was modeling the cylinder, piston, valves, and flow volume in SolidWorks 17 as described in Chapter II. The flow volume parasolid was imported into CFX as the base material and all other bodies as slices into this volume. Meshing was conducted using a fine mesh with minimum element size of 0.0002 m (0.0079 in). The curvature normal angle was set at 8 degrees. In order to provide a finer parsing around areas of particular interest, two inflations were added. At the inside of the inlet slots, a smooth transition inflation and with 9 layers and a growth rate of 1.2 was inserted. Another inflation was added at the inside wall of the cylinder with 13 total layers, a growth rate of 1.2 and a total thickness of 0.0125cm (0.0049 in). Once generated, Case 1 included 387,778 nodes, Case 2 had 396,436 nodes and Case 3 included 383,986 nodes.

2. Solver Constraints

The next step was determining the constraints of the CFX solver. Named selections were added at the inlet of the flow volume and the four exhaust ports (“Inlet” and “Outlet”

respectively). These selections were specified as boundaries with an inlet relative pressure of 27.6 kPa (4.00 psi), outlet total pressure of 0 kPa (0 psi) with an ambient total temperature of 300 K (540 R) and a reference pressure of 101.3 kPa (14.7 psi). Air, modeled as an ideal gas, was used as the fluid. Of note, actual cylinders would include diesel fuel in the flow but this analysis was conducted on air alone due to constraints of the software. In order to achieve a confident set of solutions, Solver Control was set to a k-epsilon turbulence model with artificial velocity, 2000 time steps and a residual target of 0.00001.

Convergence was based on the residuals for seven separate values: mass, momentum in three dimensions, heat energy, turbulent kinetic energy, and dissipation. Each case reached a reasonable residual for convergence after 2,000 time steps or less; Case 2 converged after 1491 time steps. Final RMS residuals are shown in Table 4.

Table 4. RMS Residual Values

Parameter	**Symbol**	**Case 1**	**Case 2**	**Case 3**
X Momentum	U	3.8e-5	7.9e-6	3.7e-4
Y Momentum	V	3.6e-5	7.5e-6	4.4e-4
Z Momentum	W	3.1e-6	5.5e-7	4.1e-4
Mass	P	4.0e-5	7.2e-6	2.8e-5
Heat Energy	H	4.9e-5	1.0e-5	6.6e-4
Turbulent Kinetic Energy	K	2.5e-5	7.0e-6	3.2e-4
Dissipation	E	5.1e-5	1.8e-5	5.4e-4

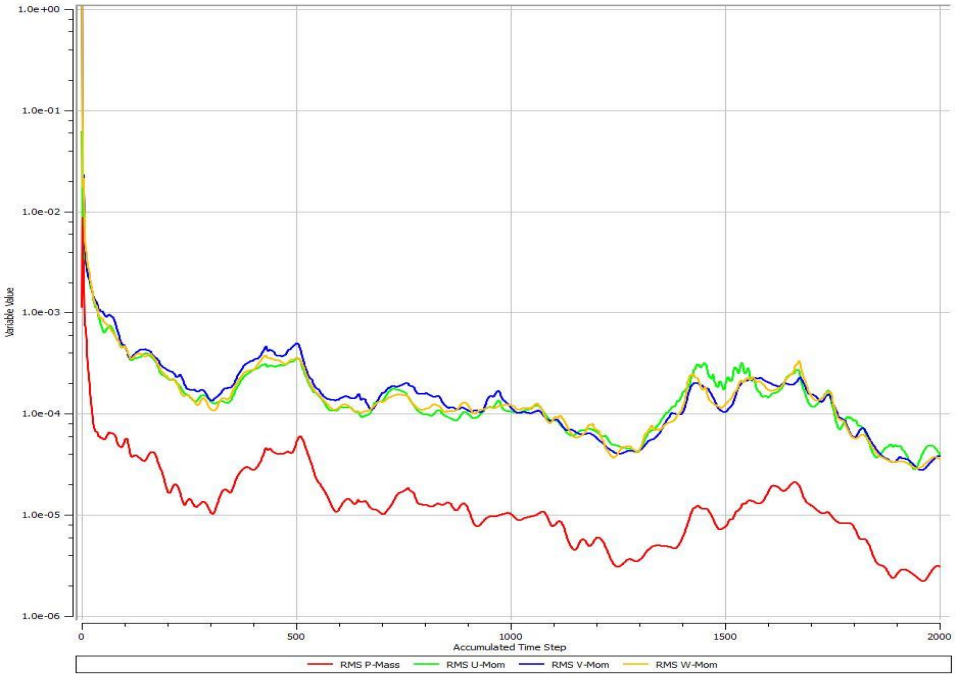

Figure 15. Momentum Display Monitors for Case 1

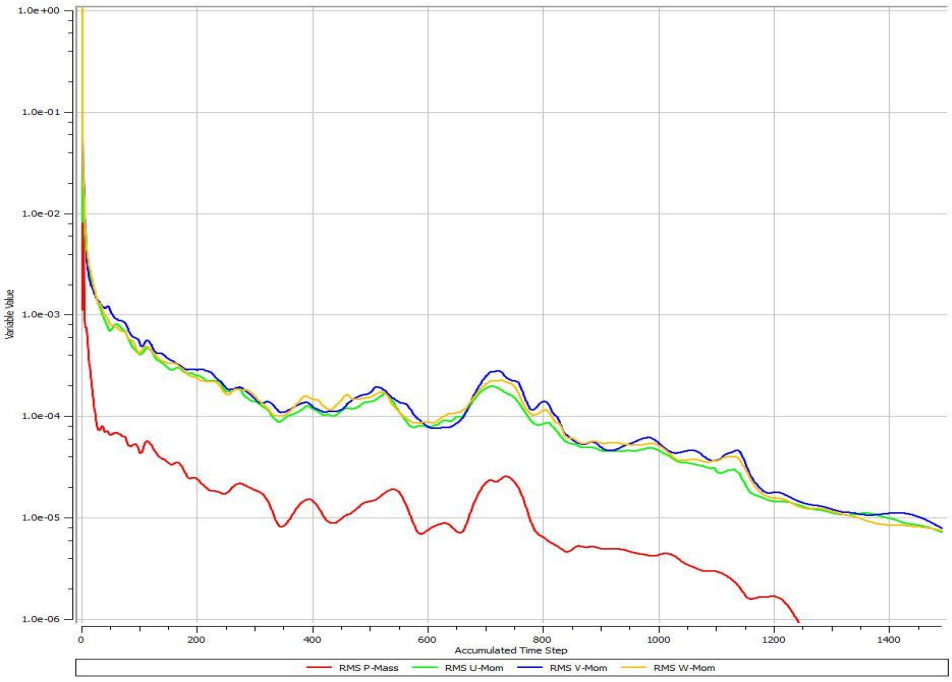

Figure 16. Momentum Display Monitors for Case 2

Figure 17. Momentum Display Monitors for Case 3

The trends shown in Figure 17 set Case 3 apart from the other two. The difference in convergence patterns indicate that the flow characteristics for this case are different than Case 1 or 2. As discussed in the following section, the different recirculation currents created by the relaxed horizontal angle are the likely culprit for the higher residual values found in Case 3. Higher residuals point to an unsteady flow, reasonable for the case with less of an induced vertex.

Since the minimums are not consistent throughout, it is reasonable to assume that the orientation of the inlet hole makes a measurable difference in the flow patterns. Also, the fact that Case 1 and 3 reach minimum residuals prior to the final time step shows a tendency toward possible unsteady flow.

B. RESULTS

1. Mass Flow Rate

Results for mass flow rate were the first parameter analyzed using the Function Calculator of CFX. Case 1 had a value of 0.271 kg/s (2151 lb/hr), Case 2 0.263 kg/s (2087

lb/hr) and Case 3 0.272 kg/s (2158.8 lb/hr). While these numbers represent minimal variance, it is worth noting that Case 2 had the lowest value, indicating the highest flow resistance. Visual comparison of the velocity vectors for each case showed similar patterns with maxima in the inlet holes and exhaust ports. Streamline analysis showed counterclockwise flow (viewed from above) inside the cylinder in each case. Air flow outside the cylinder showed a tendency to proceed farther in the clockwise direction around the outside of the cylinder, as shown in Figure 18.

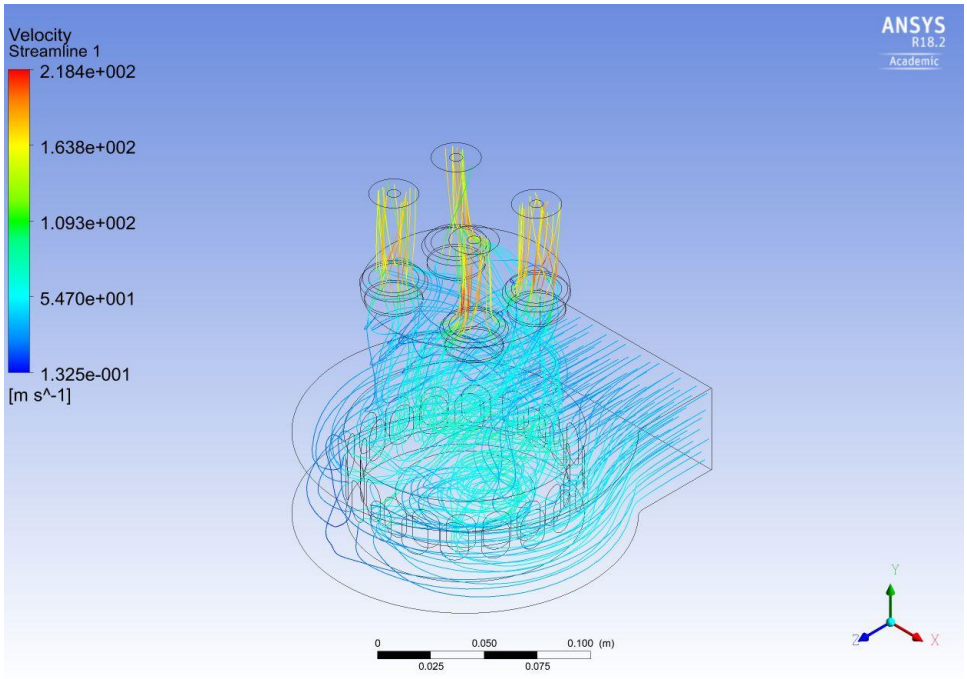

Figure 18. Velocity Streamlines for Case 1

The most viable explanation for this phenomenon is that the internal flow rotation acts as a rotating cylinder that moves the stagnation and detachment point of flow off of the centerline. Cases 2 and 3 showed similar patterns.

2. Mixing

A subjective comparison of mixing was considered. Since no actual mixing value exists for comparison in CFX and the fluid model was developed using only air, the best

measure of mixing would be the strength of swirl within the cylinder, or the "velocity swirl strength" variable.

The distinctive swirl patterns for each case are clearly depicted in Figure 19, 20 and 21. In Case 1, the swirl is more evenly distributed throughout the cylinder. Inlet slot areas show a higher value but overall the cylinder has a more uniform hue, indicating well-dispersed swirl. Case 2 shows a sharper distinction between the top, bottom, and middle of the cylinder. The top and bottom areas have higher swirl values while the area midway between TDC and BDC has minimal values. This effect is likely due to the fact that the increased vertical angle gives the air a more direct path through the cylinder and reducing the amount of circumferential motion it experiences on the way to the outlet. Case 3 displays the effect of the reduced horizontal angle: the swirl is concentrated more toward the center of the cylinder. Overall, swirl is the least in this case as well as evidenced by the high amount of blue zero-swirl area in Figure 21. Noticeably, however, Case 3 displays the highest measure of swirl around the inlet slots. Since the flow is directed away from the cylinder wall and piston head, this case is more susceptible to flow separation and the development of recirculation currents in those areas.

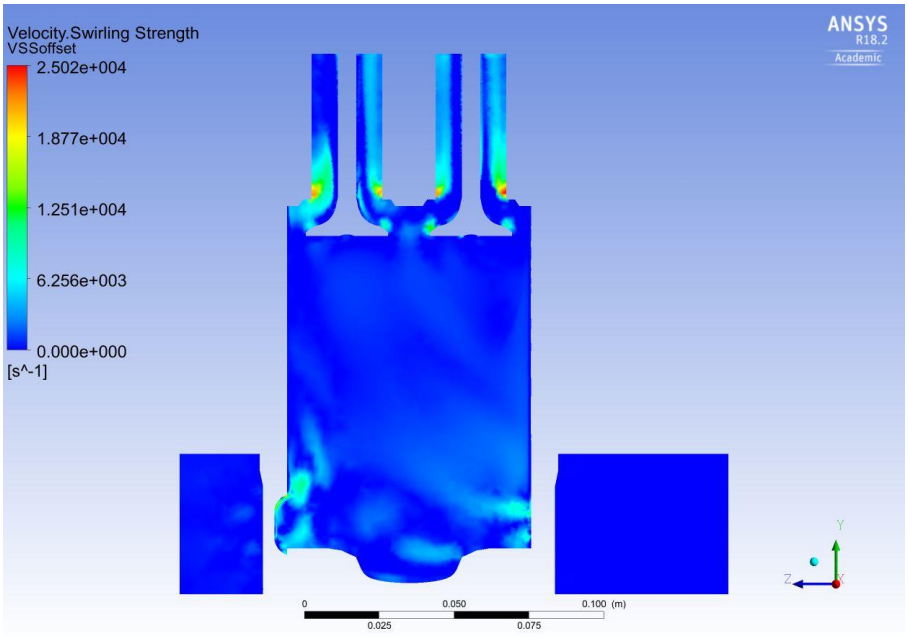

Figure 19. Velocity Swirl Strength in YZ plane for Case 1

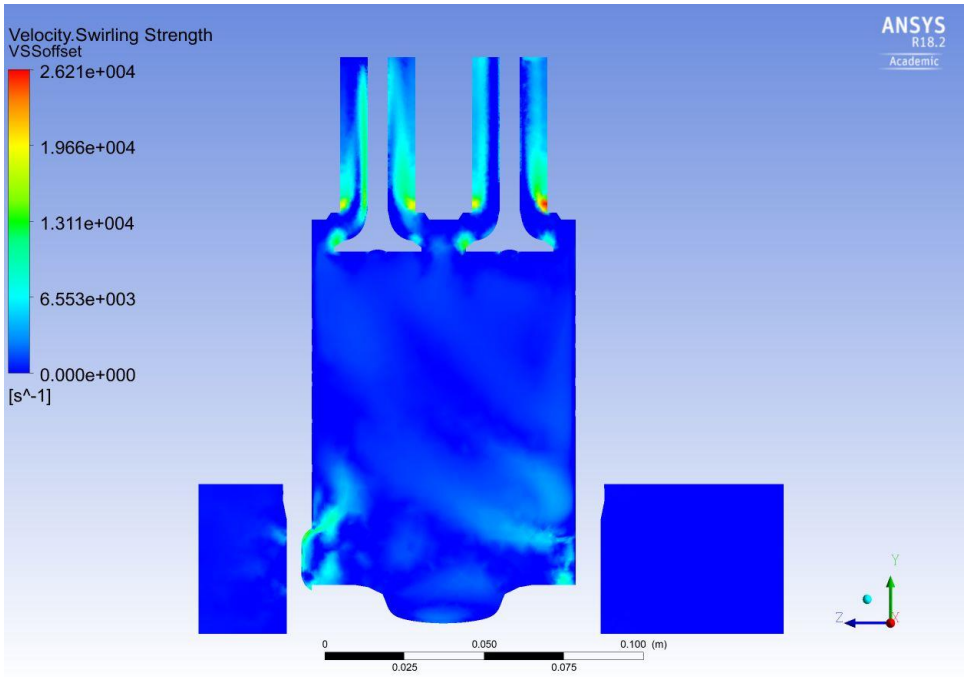

Figure 20. Velocity Swirl Strength in YZ plane for Case 2

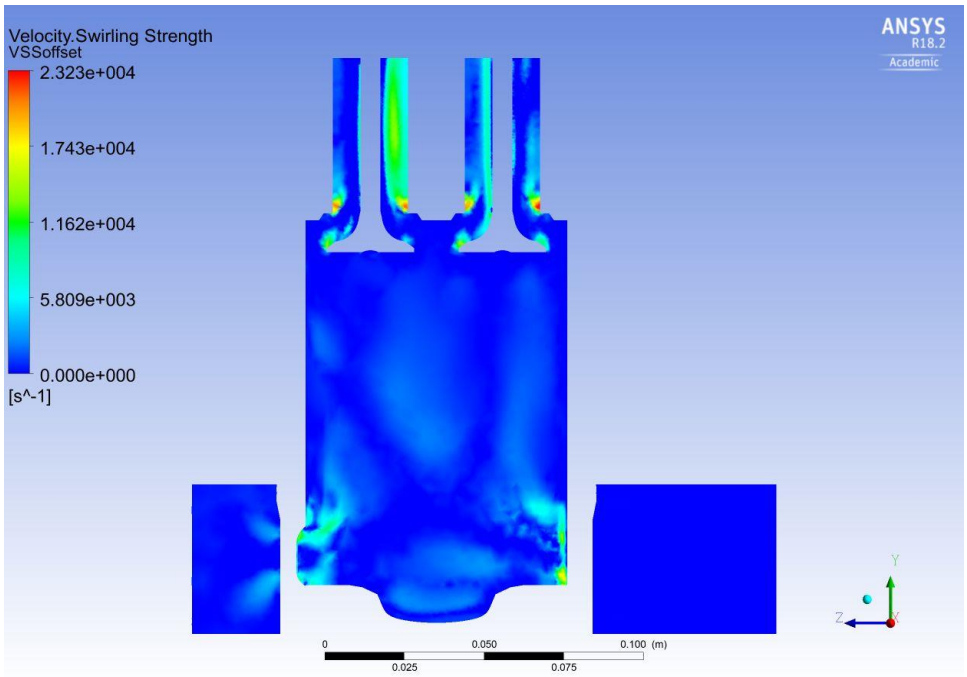

Figure 21. Velocity Swirl Strength in YZ plane for Case 3

In the XZ plane, the difference in swirl patterns is more readily visible. In Figure 22 Case 1 shows signs of a swirl distributed around the horizontal plane aligned with the inlet slots, which is reasonable considering that airflow is directed along that plane. Case 2 shows a smaller distribution of swirl strength in the XZ plane. Since the airflow enters the cylinder at a vertical angle, the higher swirl values will occur in the area above the plane shown in Figure 23. There is also a noticeably higher distribution of swirl immediately inside the inlet holes, likely due to recirculation at the bottom of the cylinder generated by the upward angle of the holes. Case 3 exhibits even higher swirl distribution between the inlets. Since the airflow in this case is directed further from the cylinder walls, the flow is more likely to detach and develop recirculation currents. Figure 24 also illustrates how the swirl is less concentrated due to flow being oriented more toward the center of the cylinder.

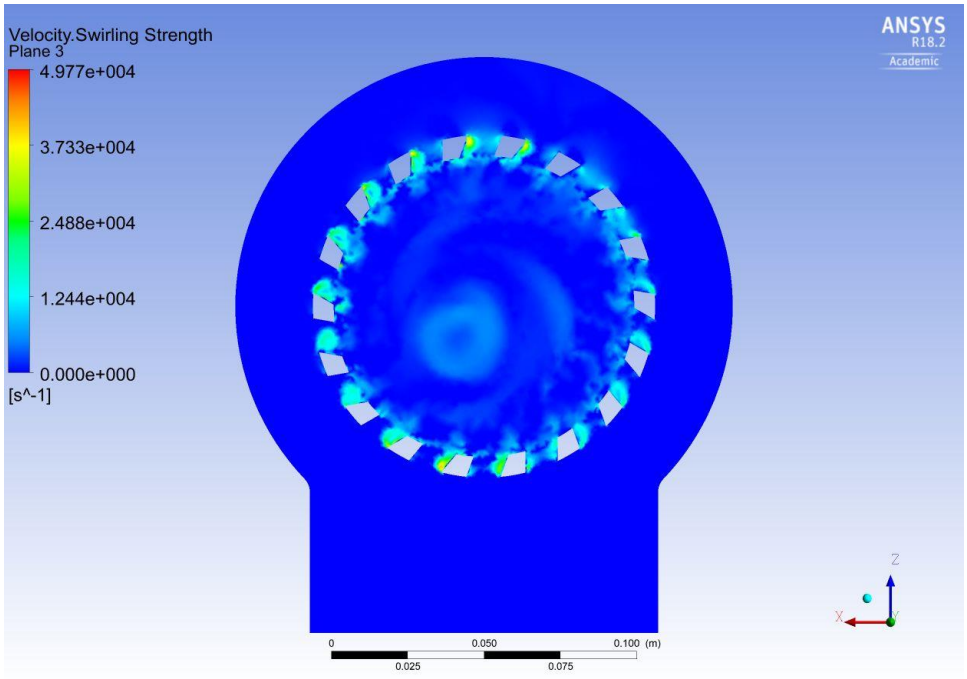

Figure 22. Velocity Swirl Strength in XZ Plane for Case 1

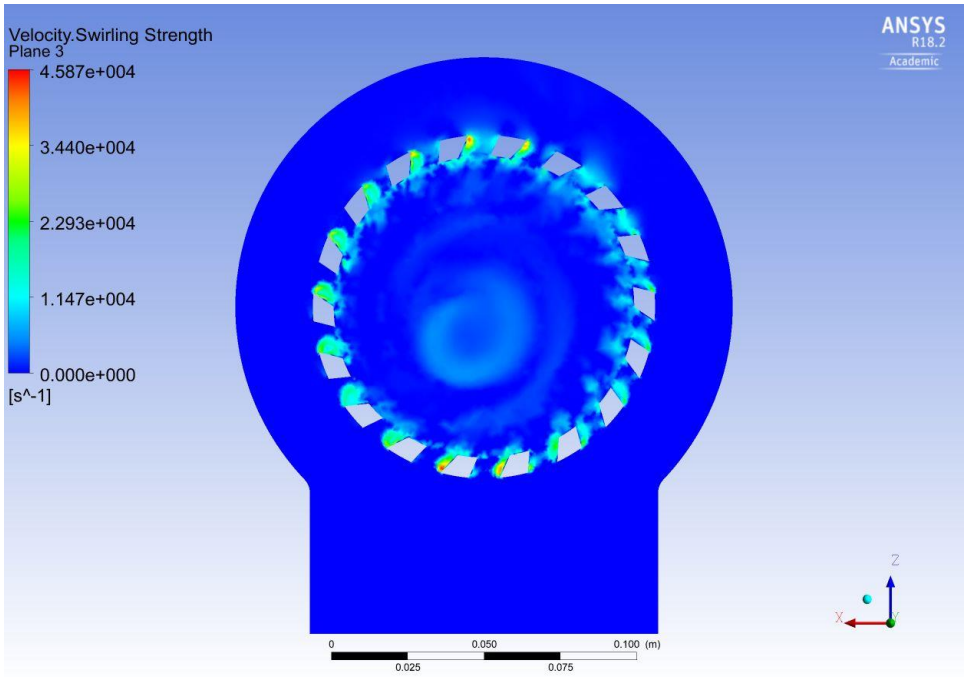

Figure 23. Velocity Swirl Strength in XZ Plane for Case 2

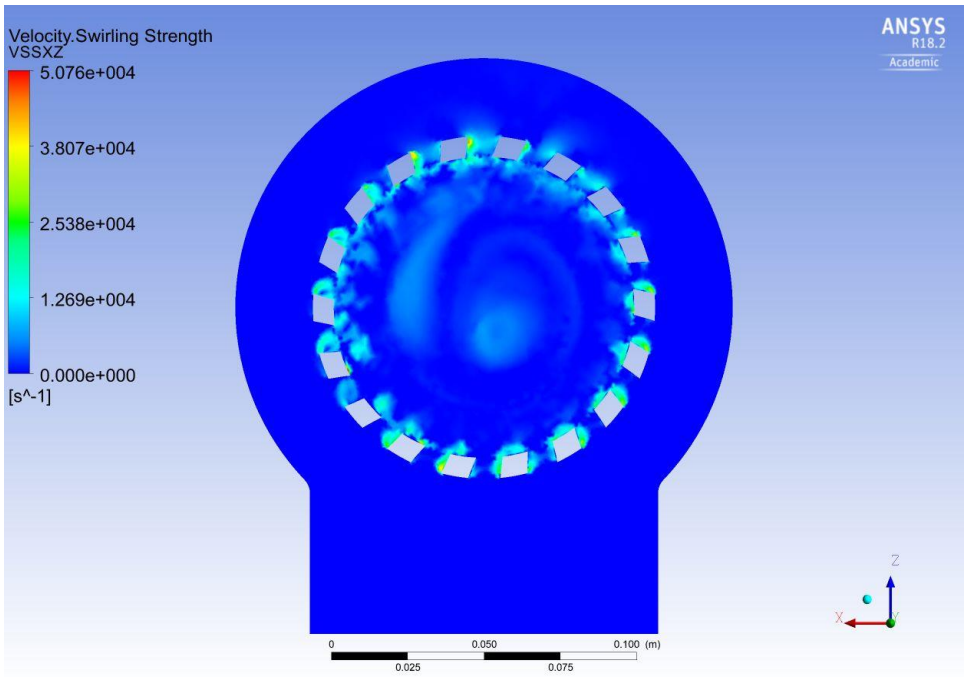

Figure 24. Velocity Swirl Strength in XZ Plane for Case 3

A three-dimensional analysis of velocity swirl strength in Figures 25, 26 and 27 reinforces the concepts highlighted above. Case 1 shows the highest dispersion while Case 2 displays higher values at the top and bottom of the cylinder. Case 3 again shows higher localized swirl at the inlet area.

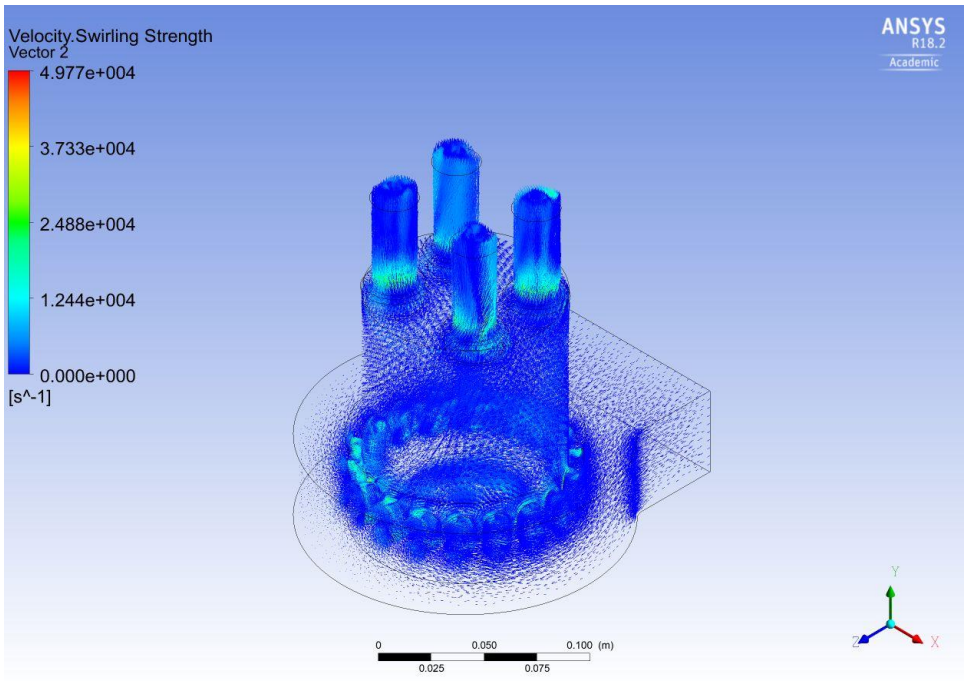

Figure 25. Velocity Swirl Strength Vectors for Case 1

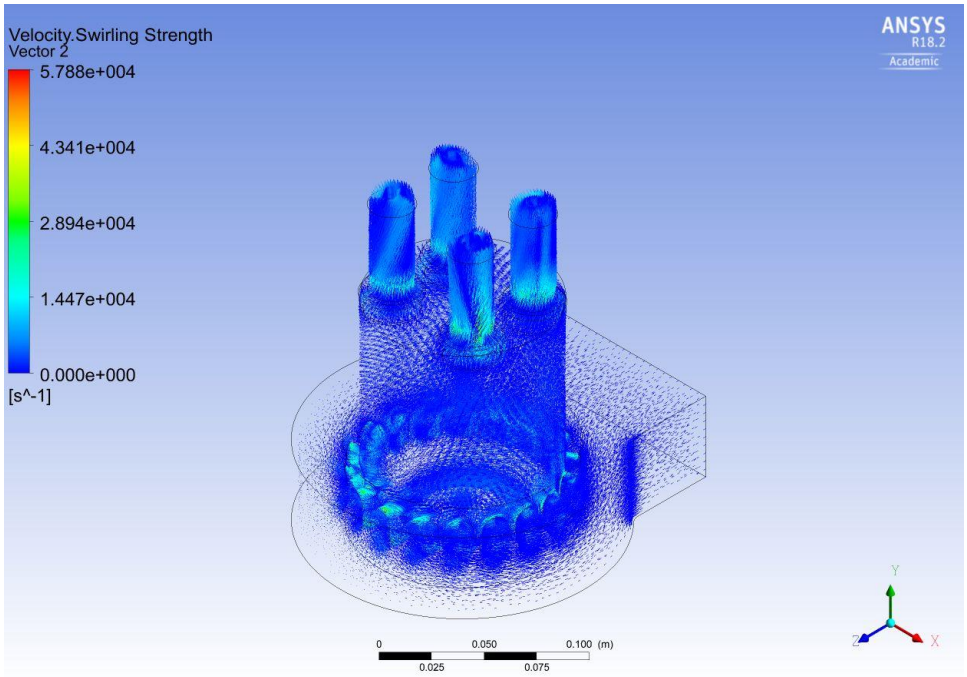

Figure 26. Velocity Swirl Strength Vectors for Case 2

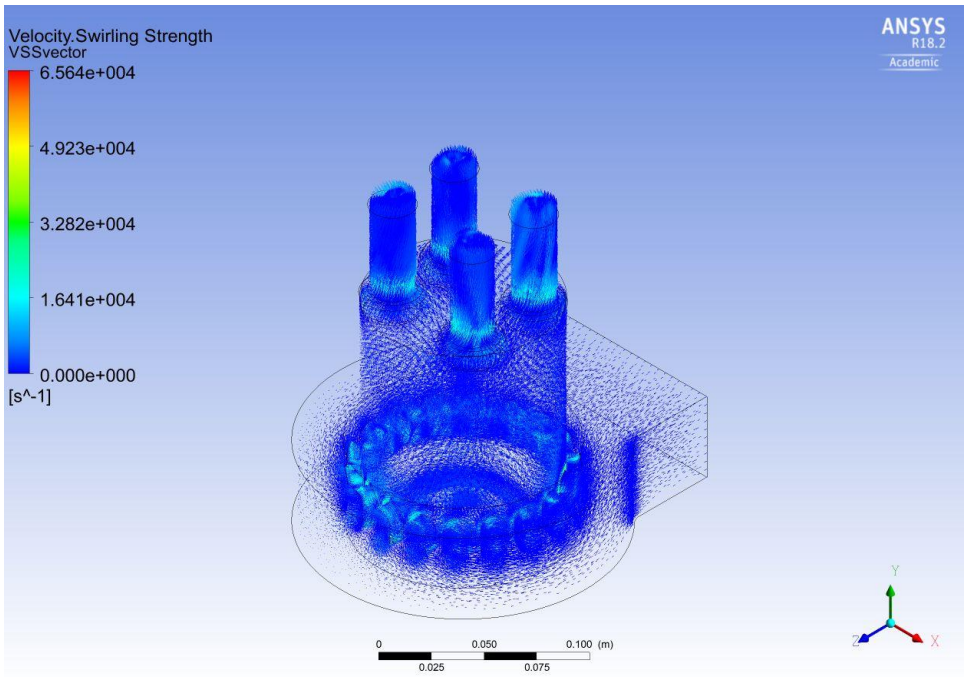

Figure 27. Velocity Swirl Strength Vectors for Case 3

3. Pressure Ratio

The final parameter of comparison was outlet to inlet static pressure ratio, averaged by mass flow rate. Case 3 had the highest ratio at 0.00124, while Case 2 was lowest at 0.00119. Case 1 fell in between at 0.00122. Case 2's lower ratio indicates a higher pressure differential or blockage through the cylinder, in keeping with the lower mass flow rate of this configuration. This quality could prove beneficial by virtue of the fact that air driven more forcefully through the cylinder will reach and mix with the fuel spray more quickly, in turn providing a better air-fuel mixture for combustion.

Pressure contours, shown in Figures 28, 29 and 30, were similar for each case with maximum pressures at the inlet and minimums at the outlet, consistent with the higher velocity/lower area values at the outlet.

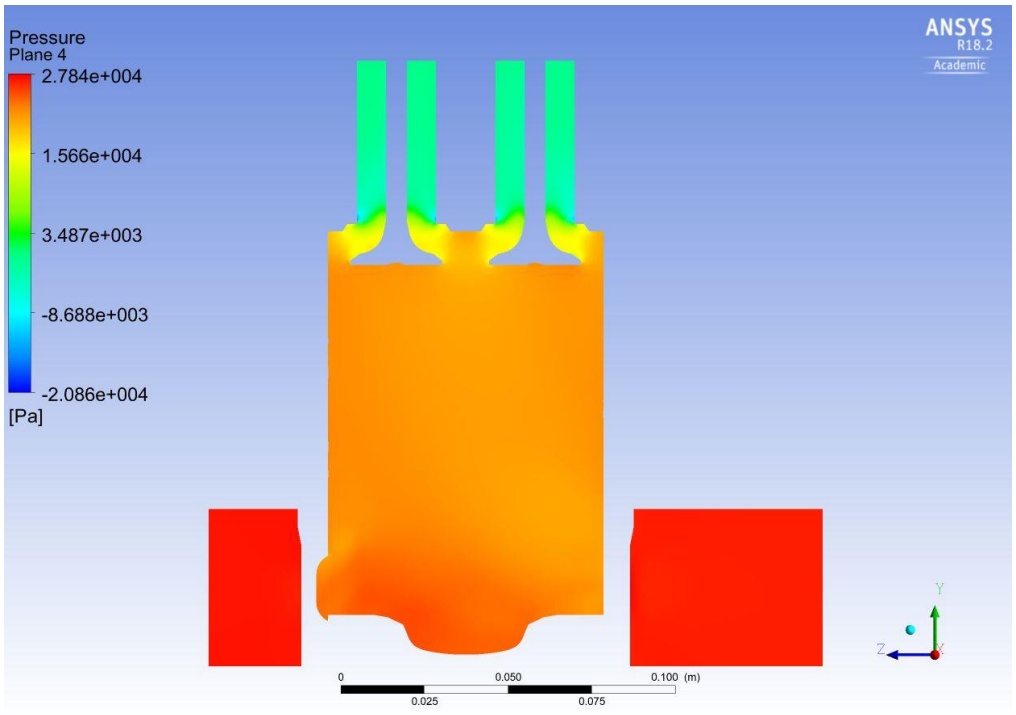

Figure 28. Vertical Pressure Contour for Case 1

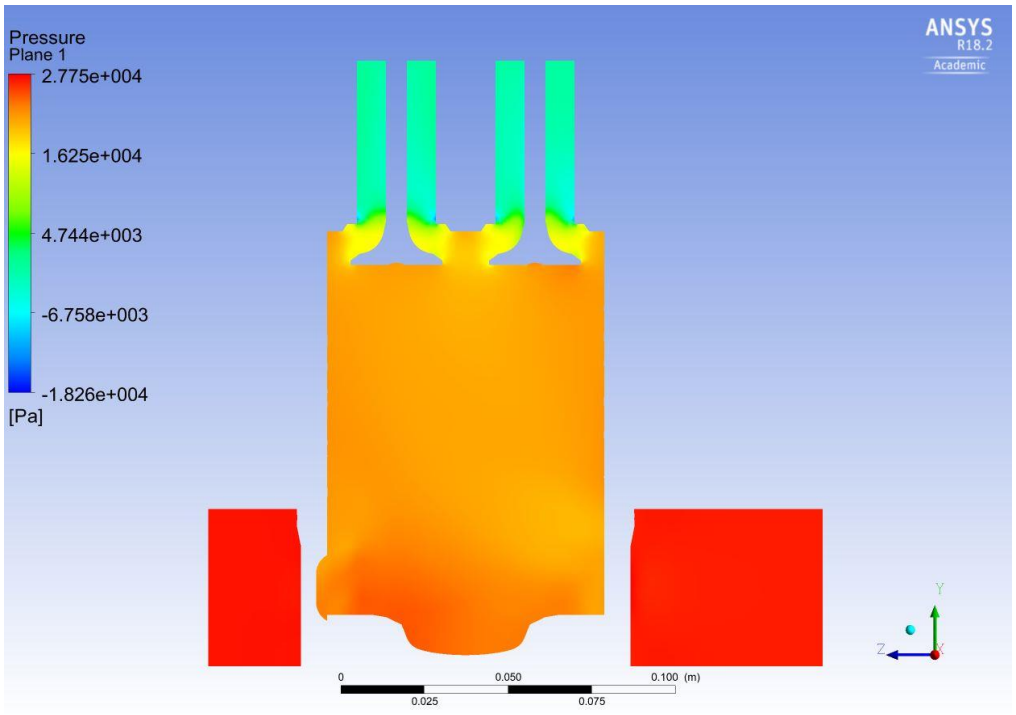

Figure 29. Vertical Pressure Contour for Case 2

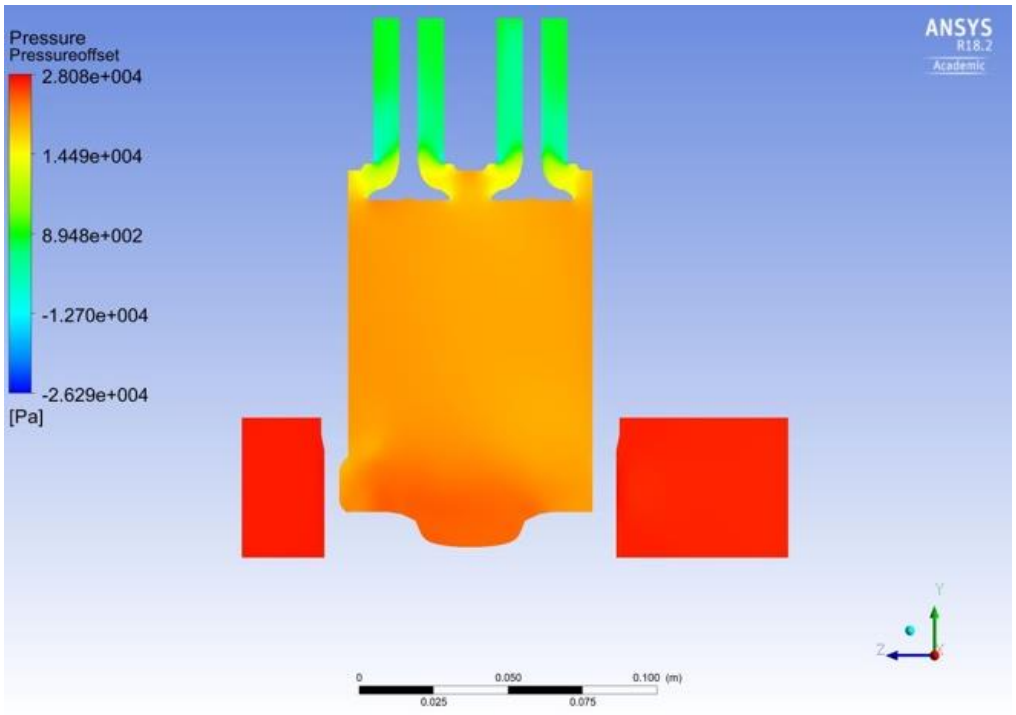

Figure 30. Vertical Pressure Contour for Case 3

C. COMPARISON

While empirical testing will ultimately show which inlet orientation provides the highest efficiency and power values for the 3-53, comparing each case by mass flow, swirl strength and pressure ratio gives excellent insight into the behavior of fluid flow in the cylinder. Throughout the analysis, Case 2 showed the highest resistance to flow. In terms of swirl, each case showed different patterns that could potentially increase mixing. Case 1 showed the most swirl dispersion in plane with the inlet slots. In contrast, Case 2 showed more concentrated swirl toward the top and bottom of the cylinder and introduced a vertical component. Case 3 demonstrated less dispersed swirl but exhibited higher values near the slots themselves and consistently showed lower flow resistance. As a result, it had higher flow rate and lower swirl. The likely cause is that the relaxed rightward angle directs the flow toward the center of the cylinder and away from wall interference. Case 2 is the most promising orientation for increased performance; higher swirl dispersion near the top of the cylinder combined with lower flow rate should result in a richer, more uniformly distributed mixture at TDC and in turn more efficient combustion. However, empirical testing is necessary to fully validate which swirl patterns and flow rates yield the best performance of the Detroit Diesel 3-53.

V. CONCLUSIONS

The baseline performance and flow characteristics studied in this thesis strongly suggest that further improvement in efficiency of the Detroit Diesel 3-53 is achievable.

Analysis of the actual performance characteristics of the NPS Marine Propulsion diesel engine show how the particular installation and configuration of the model differentiate its operation from the supplied values. Mechanical losses such as friction and incomplete combustion cause lower power and torque output at higher speeds while output at lower speeds compares more favorable to the supplied curves. Fuel and air consumption also increases at higher speeds as the mechanical efficiency of the actual engine dwindles, highlighting the importance of developing methods to incite more effective combustion. Thermal efficiency values were comparable, showing that the NPS engine was operating in accordance with the correct thermodynamic cycle. Pressure-volume analysis gave a clearer picture of how midrange speeds around 2200 RPM provide the most work per cycle.

Computational fluid analysis of the three intake hole configurations provided promising information on the airflow patterns within the cylinder. The baseline arrangement gave the most uniform swirl. Cases 2 and 3, however, provided higher and more localized swirl values. For an engine with fuel injection at the top of the cylinder, these localized areas of swirl could provide a better air-fuel mixture. The lower flow rate of case 2 offers the opportunity for air to spend more time in the cylinder mixture area as well as more time for complete combustion. Most important, however, is that the effects of inlet angle on airflow have been recorded for correlation with empirical testing.

A number of potential areas for future work exist to further improve the accuracy of the simulation and expand the scope of the analysis. The most achievable and productive addition would be to impose piston movement throughout the simulation, since an actual diesel engine cylinder is not a static volume. Adding combustion would also be a more realistic scenario but is limited by the capabilities of the software; combustion modeling in CFX has not proven reliable for air. Adding additional vertical and horizontal angle to the inlet orientation would help to more solidly correlate the effects of angling flow toward or

away from the center of the cylinder. Exhaust gas analysis would provide vital data on fuel consumption and burn rate efficiency for comparison among different test designs. The most important area for future research, however, is in empirical testing of different intake alignments. Experimental data to correlate with different flow patterns would open the door for further alteration and improvement.

Overall, the study of inlet slot angle effects on airflow is only the first step in a promising area of diesel performance enhancement.

APPENDIX. MATLAB CODE

A. SI UNITS

```
clc
clear all
close all

A=table2array(readtable('NewHeadN45560RPM30FTLB.xlsx'));
B=table2array(readtable('NewHeadN451600RPM199FTLB.xlsx'));
C=table2array(readtable('NewHeadN452200RPM180FTLB.xlsx'));
D=table2array(readtable('NewHeadN452500RPM156FTLB.xlsx'));
E=table2array(readtable('NewHeadN452600RPM140FTLB.xlsx'));

b = 9.8425; %bore
s = 11.430; %stroke
a = s/2; %crank radius
L = 22.352; %connecting rod length
Vc = 43.5420678; %Clearance volume
WA=zeros(3,3);
WB=zeros(3,3);
WC=zeros(3,3);
WD=zeros(3,3);
WE=zeros(3,3);

%% 560 RPM
A(:,2:4)=A(:,2:4)*6.89476;
Atheta = A(:,1);
AH = a*cosd(Atheta)+sqrt(L^2-a^2*sind(Atheta).^2)-(L-a);
AV = Vc + pi*(b/2)^2*(s-AH);
A(:,5) = AV;

[resA,indA]=min(AV);
for i=1:3;
    WA(1,i)=trapz(AV(1:indA),A(1:indA,i+1))/100^3;
    WA(2,i)=trapz(AV(indA:719),A(indA:719,i+1))/100^3;
    WA(3,i)=(WA(2,i)+WA(1,i));
end;
PA=sum(WA(3,:))*560/60;
disp(WA)
disp(PA)

figure(1)
plot(A(:,5),A(:,2))
hold on
plot(A(:,5),A(:,3))
plot(A(:,5),A(:,4))
xlabel('Volume (cm^3)')
ylabel('Average Cylinder Pressure (kPa)')
legend('Cylinder 1','Cylinder 2','Cylinder 3')
title('P-V Diagram at 560 RPM and 30 ft-lb')
```

```
%% 1600 RPM
B(:,2:4)=B(:,2:4)*6.89476;
Btheta = B(:,1);
BH = a*cosd(Btheta)+sqrt(L^2-a^2*sind(Btheta).^2)-(L-a);
BV = Vc + pi*(b/2)^2*(s-BH);
B(:,5) = BV;

[resB,indB]=min(BV);
for i=1:3;
    WB(1,i)=trapz(BV(1:indB),B(1:indB,i+1))/100^3;
    WB(2,i)=trapz(BV(indB:719),B(indB:719,i+1))/100^3;
    WB(3,i)=(WB(2,i)+WB(1,i));
end;
PB=sum(WB(3,:))/60*1600;
disp(WB);
disp(PB);

figure(2)
plot(B(:,5),B(:,2))
hold on
plot(B(:,5),B(:,3))
plot(B(:,5),B(:,4))
xlabel('Volume (cm^3)')
ylabel('Average Cylinder Pressure (kPa)')
legend('Cylinder 1','Cylinder 2','Cylinder 3')
title('P-V Diagram at 1600 RPM and 199 ft-lb')

%% 2200 RPM
C(:,2:4)=C(:,2:4)*6.89476;
Ctheta = C(:,1);
CH = a*cosd(Ctheta)+sqrt(L^2-a^2*sind(Ctheta).^2)-(L-a);
CV = Vc + pi*(b/2)^2*(s-CH);
C(:,5) = BV;

[resC,indC]=min(CV);
for i=1:3;
    WC(1,i)=trapz(CV(1:indC),C(1:indC,i+1))/100^3;
    WC(2,i)=trapz(CV(indC:719),C(indC:719,i+1))/100^3;
    WC(3,i)=(WC(2,i)+WC(1,i));
end;
PC=sum(WC(3,:))/60*2200;
disp(WC)
disp(PC)

figure(3)
plot(C(:,5),C(:,2))
hold on
plot(C(:,5),C(:,3))
plot(C(:,5),C(:,4))
xlabel('Volume (cm^3)')
ylabel('Average Cylinder Pressure (kPa)')
legend('Cylinder 1','Cylinder 2','Cylinder 3')
title('P-V Diagram at 2200 RPM and 180 ft-lb')
```

```
%% 2500 RPM
D(:,2:4)=D(:,2:4)*6.89476;
Dtheta = D(:,1);
DH = a*cosd(Dtheta)+sqrt(L^2-a^2*sind(Dtheta).^2)-(L-a);
DV = Vc + pi*(b/2)^2*(s-DH);
D(:,5) = DV;

[resD,indD]=min(DV);
for i=1:3;
    WD(1,i)=trapz(DV(1:indD),D(1:indD,i+1))/100^3;
    WD(2,i)=trapz(DV(indD:719),D(indD:719,i+1))/100^3;
    WD(3,i)=(WD(2,i)+WD(1,i));
end;
PD=sum(WD(3,:))/60*2500;
disp(WD);
disp(PD);

figure(4)
plot(D(:,5),D(:,2))
hold on
plot(D(:,5),D(:,3))
plot(D(:,5),D(:,4))
xlabel('Volume (cm^3)')
ylabel('Average Cylinder Pressure (kPa)')
legend('Cylinder 1','Cylinder 2','Cylinder 3')
title('P-V Diagram at 2500 RPM and 156 ft-lb')

%% 2600 RPM
E(:,2:4)=E(:,2:4)*6.89476;
Etheta = E(:,1);
EH = a*cosd(Etheta)+sqrt(L^2-a^2*sind(Etheta).^2)-(L-a);
EV = Vc + pi*(b/2)^2*(s-EH);
E(:,5) = EV;

[resE,indE]=min(EV);
for i=1:3;
    WE(1,i)=trapz(EV(1:indE),E(1:indE,i+1))/100^3;
    WE(2,i)=trapz(EV(indE:719),E(indE:719,i+1))/100^3;
    WE(3,i)=(WE(2,i)+WE(1,i));
end;
PE=sum(WE(3,:))/60*2600;
disp(WE);
disp(PE);

figure(5)
plot(E(:,5),E(:,2))
hold on
plot(E(:,5),E(:,3))
plot(E(:,5),E(:,4))
xlabel('Volume (cm^3)')
ylabel('Average Cylinder Pressure (kPa)')
legend('Cylinder 1','Cylinder 2','Cylinder 3')
title('P-V Diagram at 2600 RPM and 140 ft-lb')
```

```
%% Comparison

figure(6)
plot(A(:,5),A(:,2))
hold on
plot(B(:,5),B(:,2))
plot(C(:,5),C(:,2))
plot(D(:,5),D(:,2))
plot(E(:,5),E(:,2))
xlabel('Volume (cm^3)')
ylabel('Average Cylinder Pressure (kPa)')
legend('560 RPM','1600 RPM','2200 RPM','2500 RPM','2600RPM')

%% Curves
%
% F=table2array(readtable('Run03272018.xlsx'));
%
% figure (6)
% title('Power and Torque vs. Speed')
% xlabel('Speed (RPM)')
% yyaxis left
% plot(F(:,3),F(:,4))
% ylabel('Power (HP)')
% yyaxis right
% plot(F(:,3),F(:,5))
% ylabel('Torque (ft-lb)')
```

B. ENGLISH UNITS

```
clc
clear all
close all

A=table2array(readtable('NewHeadN45560RPM30FTLB.xlsx'));
B=table2array(readtable('NewHeadN451600RPM199FTLB.xlsx'));
C=table2array(readtable('NewHeadN452200RPM180FTLB.xlsx'));
D=table2array(readtable('NewHeadN452500RPM156FTLB.xlsx'));
E=table2array(readtable('NewHeadN452600RPM140FTLB.xlsx'));

b = 3.875; %bore
s = 4.5; %stroke
a = s/2; %crank radius
L = 8.8; %connecting rod length
Vc = 2.6571; %Clearance volume
WA=zeros(3,3);
WB=zeros(3,3);
WC=zeros(3,3);
WD=zeros(3,3);
WE=zeros(3,3);

%% 560 RPM
```

```
Atheta = A(:,1);
AH = a*cosd(Atheta)+sqrt(L^2-a^2*sind(Atheta).^2)-(L-a);
AV = Vc + pi*(b/2)^2*(s-AH);
A(:,5) = AV;

[resA,indA]=min(AV);
for i=1:3;
    WA(1,i)=trapz(AV(1:indA),A(1:indA,i+1))/23760000;
    WA(2,i)=trapz(AV(indA:719),A(indA:719,i+1))/23760000;
    WA(3,i)=(WA(2,i)+WA(1,i));
end;
PA=sum(WA(3,:))*60*560;
disp(WA)
disp(PA)

figure(1)
plot(A(:,5),A(:,2))
hold on
plot(A(:,5),A(:,3))
plot(A(:,5),A(:,4))
xlabel('Volume (in^3)')
ylabel('Average Cylinder Pressure (psi)')
legend('Cylinder 1','Cylinder 2','Cylinder 3')
title('P-V Diagram at 560 RPM and 30 ft-lb')

%% 1600 RPM

Btheta = B(:,1);
BH = a*cosd(Btheta)+sqrt(L^2-a^2*sind(Btheta).^2)-(L-a);
BV = Vc + pi*(b/2)^2*(s-BH);
B(:,5) = BV;

[resB,indB]=min(BV);
for i=1:3;
    WB(1,i)=trapz(BV(1:indB),B(1:indB,i+1))/23760000;
    WB(2,i)=trapz(BV(indB:719),B(indB:719,i+1))/23760000;
    WB(3,i)=(WB(2,i)+WB(1,i));
end;
PB=sum(WB(3,:))*60*1600;
disp(WB);
disp(PB);

figure(2)
plot(B(:,5),B(:,2))
hold on
plot(B(:,5),B(:,3))
plot(B(:,5),B(:,4))
xlabel('Volume (in^3)')
ylabel('Average Cylinder Pressure (psi)')
legend('Cylinder 1','Cylinder 2','Cylinder 3')
title('P-V Diagram at 1600 RPM and 199 ft-lb')

%% 2200 RPM
```

```
Ctheta = C(:,1);
CH = a*cosd(Ctheta)+sqrt(L^2-a^2*sind(Ctheta).^2)-(L-a);
CV = Vc + pi*(b/2)^2*(s-CH);
C(:,5) = BV;

[resC,indC]=min(CV);
for i=1:3;
    WC(1,i)=trapz(CV(1:indC),C(1:indC,i+1))/23760000;
    WC(2,i)=trapz(CV(indC:719),C(indC:719,i+1))/23760000;
    WC(3,i)=(WC(2,i)+WC(1,i));
end;
PC=sum(WC(3,:))*60*2200;
disp(WC)
disp(PC)

figure(3)
plot(C(:,5),C(:,2))
hold on
plot(C(:,5),C(:,3))
plot(C(:,5),C(:,4))
xlabel('Volume (in^3)')
ylabel('Average Cylinder Pressure (psi)')
legend('Cylinder 1','Cylinder 2','Cylinder 3')
title('P-V Diagram at 2200 RPM and 180 ft-lb')

%% 2500 RPM

Dtheta = D(:,1);
DH = a*cosd(Dtheta)+sqrt(L^2-a^2*sind(Dtheta).^2)-(L-a);
DV = Vc + pi*(b/2)^2*(s-DH);
D(:,5) = DV;

[resD,indD]=min(DV);
for i=1:3;
    WD(1,i)=trapz(DV(1:indD),D(1:indD,i+1))/23760000;
    WD(2,i)=trapz(DV(indD:719),D(indD:719,i+1))/23760000;
    WD(3,i)=(WD(2,i)+WD(1,i));
end;
PD=sum(WD(3,:))*60*2500;
disp(WD);
disp(PD);

figure(4)
plot(D(:,5),D(:,2))
hold on
plot(D(:,5),D(:,3))
plot(D(:,5),D(:,4))
xlabel('Volume (in^3)')
ylabel('Average Cylinder Pressure (psi)')
legend('Cylinder 1','Cylinder 2','Cylinder 3')
title('P-V Diagram at 2500 RPM and 156 ft-lb')

%% 2600 RPM
```

```
Etheta = E(:,1);
EH = a*cosd(Etheta)+sqrt(L^2-a^2*sind(Etheta).^2)-(L-a);
EV = Vc + pi*(b/2)^2*(s-EH);
E(:,5) = EV;

[resE,indE]=min(EV);
for i=1:3;
    WE(1,i)=trapz(EV(1:indE),E(1:indE,i+1))/23760000;
    WE(2,i)=trapz(EV(indE:719),E(indE:719,i+1))/23760000;
    WE(3,i)=(WE(2,i)+WE(1,i));
end;
PE=sum(WE(3,:))*60*2600;
disp(WE);
disp(PE);

figure(5)
plot(E(:,5),E(:,2))
hold on
plot(E(:,5),E(:,3))
plot(E(:,5),E(:,4))
xlabel('Volume (in^3)')
ylabel('Average Cylinder Pressure (psi)')
legend('Cylinder 1','Cylinder 2','Cylinder 3')
title('P-V Diagram at 2600 RPM and 140 ft-lb')
legend('Cylinder 1','Cylinder 2','Cylinder 3')

%% Comparison

figure(6)
plot(A(:,5),A(:,2))
hold on
plot(B(:,5),B(:,2))
plot(C(:,5),C(:,2))
plot(D(:,5),D(:,2))
plot(E(:,5),E(:,2))
xlabel('Volume (in^3)')
ylabel('Average Cylinder Pressure (psi)')
legend('560 RPM','1600 RPM','2200 RPM','2500 RPM','2600RPM')

%% Curves
%
% F=table2array(readtable('Run03272018.xlsx'));
%
% figure (6)
% title('Power and Torque vs. Speed')
% xlabel('Speed (RPM)')
% yyaxis left
% plot(F(:,3),F(:,4))
% ylabel('Power (HP)')
% yyaxis right
% plot(F(:,3),F(:,5))
% ylabel('Torque (ft-lb)')
```

THIS PAGE INTENTIONALLY LEFT BLANK

LIST OF REFERENCES

[1] "Development of the two-stroke oil engine," *Journal of the American Society for Naval Engineers*, vol. 49, no. 2, pp. 241–247, Mar. 2009.

[2] K. S. B. Srinivasa and P. K. Shankaregowda, "A novel approach to a two-stroke dual stage expansion engine concept," MS thesis, Chalmers University of Technology, Gothenburg, Sweden, 2016. [Online]. Available: http://publications.lib.chalmers.se/records/fulltext/248224/248224.pdf

[3] N. W. Sung, J. A. Laitone, and D. J. Patterson, "Angled jet flow model for a diesel engine intake process—random vortex method," *International Journal for Numerical Methods in Fluids*, vol. 3, no. 3, pp. 283-293, May 1983.

[4] J. Petersen, "Combustion heat release rate comparison of algae hydroprocessed renewable diesel to F-76 in a two-stroke diesel engine,", MS thesis, Naval Postgraduate School, Monterey, CA, 2013. [Online]. Available: http://hdl.handle.net/10945/34720

[5] *Series 53 Service Manual Detroit Diesel Engines*, 9/73. Detroit, MI: Detroit Diesel, 1973.

[6] Detroit Diesel Allsion , *Engine performance curve*, Curve E4-5031-52-3, 1987.

[7] *Parts Book In-Line 53 Engines*, 5th–64th ed. Detroit, MI: Detroit Diesel Engine Division, General Motors Corporation, 1964.

THIS PAGE INTENTIONALLY LEFT BLANK

INITIAL DISTRIBUTION LIST

1. Defense Technical Information Center
   Ft. Belvoir, Virginia

2. Dudley Knox Library
   Naval Postgraduate School
   Monterey, California